New Late Cretaceous and CAMP magmatic sources off West Iberia, from high-resolution magnetic surveys on the continental shelf

Marta Neres[1,2], Pedro Terrinha[1,2], João Noiva[1], Pedro Brito[1], Marcos Rosa[1], Luis Batista[1], Carlos Ribeiro[3,4,5]

[1] IPMA - Instituto Português do Mar e da Atmosfera, 1749-077 Lisboa, Portugal

[2] Universidade de Lisboa, Faculdade de Ciências, Instituto Dom Luiz, 1749-016 Lisboa, Portugal

[3] Dep. of Geosciences, School of Science and Technology, University of Évora, Portugal

[4] ICT - Institute of Earth Sciences, University of Évora, Portugal

[5] MARE - Marine and Environmental Sciences Center, University of Évora, Portugal

Corresponding author: Marta Neres (marta.neres@ipma.pt)

Key Points:

- High-resolution magnetic data reveal a complex crustal anomaly field on the SW Iberia continental shelf, divided into distinct anomaly zones
- Magmatic intrusions are denser and larger in the Cabo Raso and Sines complexes, and other new smaller or deeper intrusions were found
- The distribution and geometry of magmatic intrusions were mainly controlled by inherited crustal tectonic fabric from the Variscan orogeny

This article has been accepted for publication and undergone full peer review but has not been through the copyediting, typesetting, pagination and proofreading process, which may lead to differences between this version and the Version of Record. Please cite this article as doi: 10.1029/2022TC007637.

Abstract

Magma-poor rifted margins can be affected by magmatic occurrences coeval with rifting and post-rifting. Understanding the geological processes that originated these magmatic events requires determining their extent, type and size of magmatic bodies and tectonics. This work investigates the distribution and origin of two large magmatic events off SW Iberia, the Late Triassic Central Atlantic Magmatic Province (CAMP) and the West Iberia Late Cretaceous Alkaline Province (WILCAP). Marine magnetic data were densely acquired over ~4400 km^2 and new magnetic maps reveal a complex heterogeneous anomaly field with different anomaly zones. A wide number and variety of magmatic bodies are interpreted, from km-scale deeply intruded plutons to small plug-like and dike-like intrusions. Integration with bathymetry and seismic reflection data allows discussing the geometry, extent and age of the magmatic sources. The Cabo Raso complex is a densely intruded zone related to the WILCAP event. The Sines complex comprises the offshore prolongation of the on-land Sines WILCAP magmatic rocks but also the newly mapped Côvo and Milfontes anomalies. Côvo is possibly the largest magmatic intrusion recognized in West Iberia. Milfontes intrudes the non-rifted Paleozoic crust and is the first known evidence of a plutonic source of the CAMP in Iberia. The intrusion of magmatic bodies was mostly controlled by the crustal tectonic fabric inherited from the Paleozoic Variscan orogeny, which was re-worked during the Mesozoic rifting and the Cenozoic Alpine collision.

Plain Abstract

The opening and closing of oceans and welding of supercontinents can be accompanied by large areas affected by magmatism unrelated to oceanic drifting implying independent geodynamic causes. We investigate the distribution of two magmatic events: the ~200 million years (Ma) Central Atlantic Magmatic Province (CAMP) and the West Iberia Late Cretaceous Alkaline Province (WILCAP) formed between 94 and 72 Ma ago. CAMP is the largest Large Igneous Province on Earth (spanning from Central Brazil to northern France), however its volcanic activity did not last more than 1 Ma. WILCAP has a much smaller extent but lasted more than 20 Ma. CAMP is represented by ~400m thick lava flows and their deep sources were only firstly reported in 2021. WILCAP is known for km-scale massifs of peculiar magmatic rocks (Sintra, Sines, Monchique) and other volcanic and intrusive rocks occurring onshore West Portugal. We present new marine magnetic maps for ~4400 km^2 that reveal complex magnetic anomalies, unraveling the cause of the Cabo Raso magnetic anomaly near Lisbon known since the 15^{th} century by Portuguese navigators for deflecting the ship compasses; discovering the Côvo buried intrusion, so far the largest off West Iberia; discovering a new deep source of the CAMP volcanism.

1. Introduction

The southwest of Iberia experienced continental rifting in Triassic-Jurassic times, associated with the opening of the North Atlantic (at west) and Neo-Tethys oceans (at south). Although both margins are magma-poor, they have been affected by three magmatic events, among which the more important and best represented are the Central Atlantic Magmatic Province (CAMP Large Igneous Province) of Late Triassic-early Jurassic age associated with the Pangea break up, and the post-rifting West Iberia Late Cretaceous Alkaline Province (WILCAP). The onshore outcropping occurrences of these events are well known and have been the focus of several studies (e.g. Font et al., 2015; Martins et al., 2008; Miranda et al., 2009; Neres et al., 2012, 2014; Ribeiro et al., 2013; Rock, 1982; Terrinha et al., 2017). On the other hand, several volcanic seamounts in distal parts of the margin have also been associated with the WILCAP (Geldmacher et al., 2006; Merle et al., 2006, 2018). However, the offshore occurrence of magmatic bodies in the continental shelf remains poorly known, except for the Estremadura Spur where studies have recently been conducted (Escada et al., 2022; Pereira et al., 2021; Simões et al., 2020). Good knowledge of the characteristics of the magmatic rocks (from direct sampling) and detailed mapping of the magmatic bodies (usually through indirect measurements) are essential to infer the origin and extent of the magmatism, its tectonic setting, and the mechanisms of intrusion. Moreover, intrusive bodies can localize brittle strain due to rheologic contrast with the surrounding crust and thus constitute seismicity clusters (e.g. Campbell, 1978). This is important for West Iberia, located close to the Nubia-Eurasia plate boundary where deformation is distributed, and rheological variations may be determinant. Note that the most active seismic cluster in mainland Portugal coincides with the WILCAP Monchique intrusion (Camargo, 2022; Custódio et al., 2015; Soares, 2018).

This work brings new information on the magmatism that affected West Iberia, particularly the CAMP and WILCAP events. We show the high potential of high-resolution magnetic surveys for discriminating and interpreting complex magnetic sources. We compile several surveys conducted on the continental shelf and unravel the

existence of unknown offshore magmatic bodies. The analysis of magnetic data is complemented by simultaneously acquired acoustic data (multibeam bathymetry and backscatter, high-resolution seismic reflection data), vintage seismic data, and geological information. This joint analysis allows interpretation of the magmatic and tectonic processes, mapping unknown offshore bodies, and establishing their relationship with onshore ones.

2. Geological setting

2.1. Main stratigraphic formations and tectonics

The study area straddles across four main tectonic units of West Portugal: the Paleozoic Variscan basement, the Mesozoic Lusitanian and Alentejo rift basins and the Cenozoic basins of Tagus and Sado Rivers (**Figure 1**).

The Variscan orogen formed as a result of oceanic subduction of the Rheic Ocean and continental collision of Gondwana and Laurasia (Nance et al., 2012). Final continental collision was reached in Permian times when Pangea supercontinent formed and the Late Variscan fracturing event occurred (Arthaud & Matte, 1977; Quesada et al., 2019). This fracturing event originated long conjugated NW-SE, NE-SW strike-slip faults that were re-worked during the Mesozoic rifting, both in the Alentejo and Lusitanian Basins. One of these faults, the ~600 km long Messejana Fault, hosts a tholeiitic basaltic dike that is part of the CAMP (de Vicente et al., 2021).

The CAMP volcanism started in the end of the Late Triassic (~203 Ma), during the early stage of the Mesozoic rifting of the West Iberia Margin (Martins et al., 2008; Marzoli et al., 1999). The Mesozoic rifting in the study area lasted until the Early Cretaceous (Aptian times, ~120 Ma) and was followed by the emplacement of the WILCAP.

The Cenozoic Tagus-Sado Rivers basins formed as foreland basins of the tectonic inversion of the Lusitanian Basin reworking the main Paleozoic and Mesozoic faults (Pais et al., 2012; Terrinha, et al., 2019a).

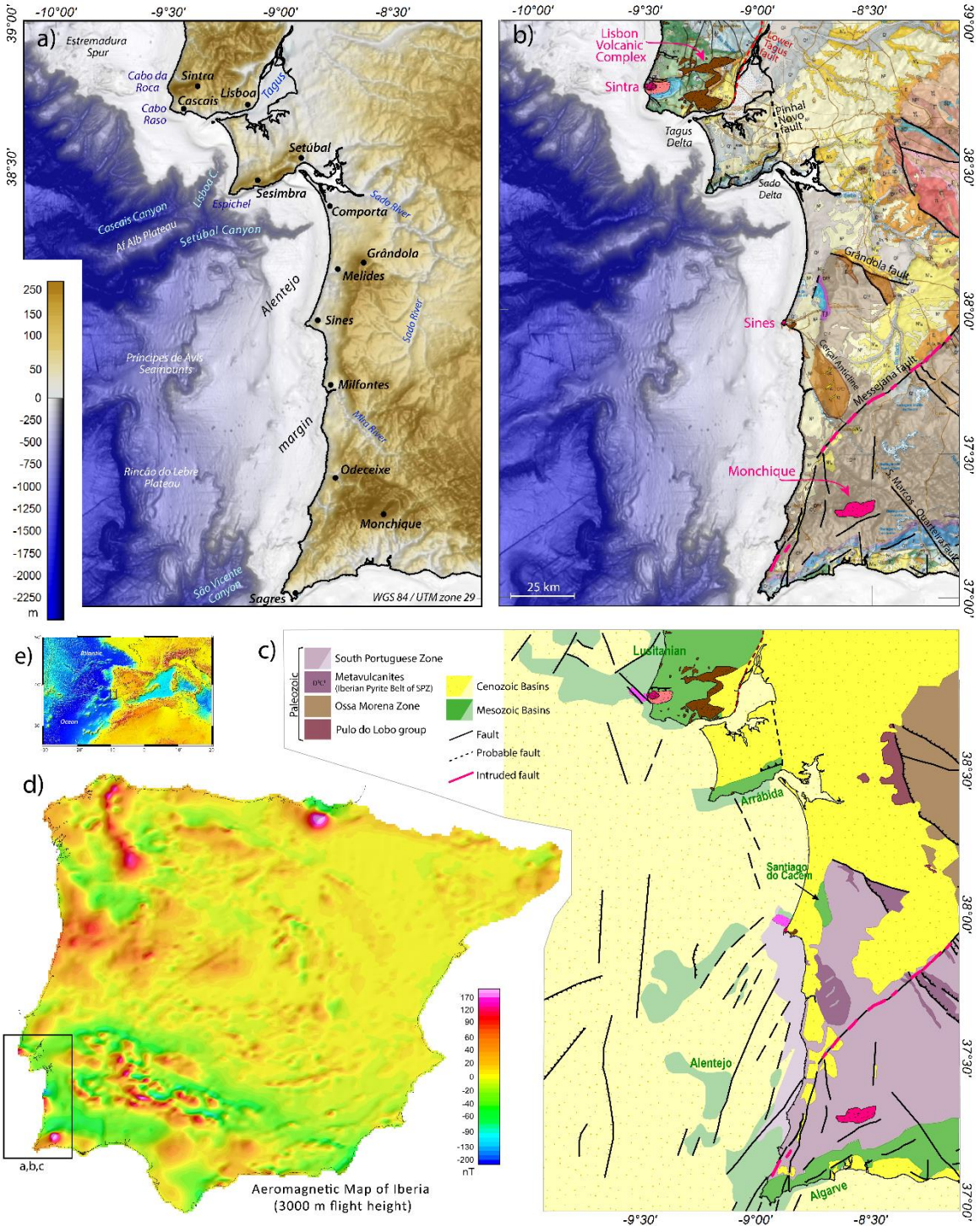

***Figure 1**: Geological setting. **(a)** Bathymetry (www.emodnet-bathymetry.eu) and topography (https://www.ngdc.noaa.gov/mgg/global/) of the study area, and main morphological features. **(b)** Onshore geological map (1:10^6; https://geoportal.lneg.pt/) shaded by topographic relief. Main faults and potential magnetic sources are highlighted: Upper Cretaceous magmatism (Lisbon volcanic complex and associated sub-volcanic dikes and sills, and Sintra, Sines and Monchique plutonic complexes) – WILCAP; Paleozoic meta-volcanic rocks of the South Portuguese zone (D^3C^1 unit); and the Hettangian (~203 Ma) Messejana basic dike - CAMP. **(c)** Simplified geological map with main onshore geological units and faults, and offshore map from **https://geoportal.lneg.pt/**. Note that results from this work will contribute to improve the offshore mapping. **(d)** Aeromagnetic map of Iberia (Ardizone et al., 1989 for Spain; Miranda et al., 1989 for Portugal; Socias & Mezcua, 2002 for compilation). **(e)** Location of Iberia in the eastern margin of the Atlantic Ocean, between Africa and Eurasia plate collision (Alpine orogeny).*

2.1.1. The Paleozoic formations

The Paleozoic crops out along 80 km of the total 150 km long coastline of the study area, namely to the south of Sines (**Figure 1**). Onshore, the Paleozoic stratigraphic record spans from Devonian through Carboniferous age formed during the Variscan orogeny that followed the Cambrian-Ordovician-Silurian rifting and passive margin stages. The basement comprises three main tectono-stratigraphic zones: the South Portuguese Zone, the Pulo do Lobo Zone and the Ossa-Morena Zone, from external to internal, respectively. The South Portuguese Zone includes the Iberian Pyrite Belt Domain of Devonian and Early Carboniferous ages and the Baixo Alentejo Flysch Domain of Carboniferous age in the greenschist to zeolite metamorphic facies. The Ossa-Morena Zone is very complex and incorporates a variety of allochthonous and autochthonous formations of sedimentary, volcano-sedimentary and plutonic affinities mostly metamorphosed in the greenschist to amphibolite facies most of them of the Lower Paleozoic and Devonian age. The Pulo do Lobo Zone is ascribed to the suture zone associated to the Lower Paleozoic subduction and collision, containing rocks of oceanic crust affinity and ophiolite remnants (Oliveira et al., 2019; Quesada et al., 2019).

The general structure is a SW-verging metamorphic thin-skinned fold and thrust belt. Deep seismic reflection profiles (Quesada et al., 2019) show the thin-skinned belt

detaching on top of a less deformed seismic unit, possibly the Lower Paleozoic, and the underlying Moho discontinuity approximately at 30 km depth. It is noteworthy that the magnetic anomalies associated to the onshore exposed Paleozoic do not exceed ~160 nT (**Figure 1**).

The Paleozoic orogenic fabric is cut by the ~W-E striking Grândola Fault, a Late Variscan right-lateral strike slip fault that was reactivated during the Cenozoic Alpine tectonics as an extensional fault (Ribeiro, 2002). The ~N-S striking left-lateral conjugate faults were reactivated as extensional faults during the Mesozoic rifting and as strike-slip faults during the Alpine compression. To the north of Sines, the Paleozoic formations (South Portuguese Zone) are covered by approximately 3 km of Mesozoic and Cenozoic sediments.

2.1.2. The Mesozoic formations

The Mesozoic sedimentary formations were deposited in the Lusitanian and Alentejo rift and post-rift basins. The rifting stages lasted from Triassic through Early Cretaceous and include a volcano-sedimentary complex of Late Triassic-Early Jurassic age, which is part of the CAMP (Marzoli et al., 1999). The post-rifting stage initiated with uplift of the Portuguese Margin associated with the emplacement of the WILCAP (**Figure 1**).

The Triassic-Hettangian volcanic-sedimentary complex that consists of red beds (mainly sandstones, marls, dolomites and basic volcanics of the CAMP) is only present onshore NE of Sines (Santiago do Cacém). The Jurassic-Cretaceous sequences are very well exposed along the Arrábida thrust and fold belt (Espichel to Setúbal in **Figure 1**). The Jurassic through Cretaceous series are mainly marine carbonate dominated facies with exception of the Upper Jurassic-Lowermost Cretaceous where the siliciclastic component can be dominant. The maximum thickness of the Lusitanian Basin Mesozoic in the study area is between 5.5 km and 6 km (Terrinha et al., 2019a). For the deep offshore part of the Alentejo Basin, Alves et al. (2009) propose a maximum total thickness of ~6km (with 2.2 km for the Upper Jurassic) based on multichannel seismic profiles. Onshore, drillings in the Upper Jurassic formations showed a total thickness of ~0.6 km, possibly a rift

shoulder equivalent. The rift faults tend to strike N-S to NE-SW with exception of the south-western part of the Lusitanian Basin where NW striking rift faults can be important.

2.1.3. The Cenozoic formations

The Cenozoic sedimentary cover of the Lower Tagus and Sado Rivers Basins overlie the southern part of the Lusitanian Basin and part of the Variscan basement. The Paleogene consists of highly heterogeneous terrigenous units deposited in subaerial environments as a result of diastrophic activity. Its maximum thickness is ~0.4 km in the Lisbon region. The Neogene consists mainly of Miocene shallow water carbonates and Pliocene red siliciclastic conglomerates and sandstones with maximum thicknesses of 800 m and 300m, respectively (Pais et al., 2012).

Onshore, south of the Grândola Fault, the Paleogene has a maximum thickness of 260 m, the Miocene of 100 m, the Pliocene of 20 m and the Quaternary of 30 m (Dias et al., 2016). In the deep offshore the whole Cenozoic can be as thick as ~2km (Alves et al., 2003, 2009). The oil industry wells Pescada-1 and Golfinho drilled through ~300 m and ~600 m of Cenozoic, respectively.

2.2. Magmatism

The West Iberia Margin hosts three Mesozoic magmatic events. The first event lasted for ~2 Ma in the Triassic-Jurassic transition (Font et al., 2015; Martins et al., 2008; Marzoli et al., 1999). It is of tholeiitic affinity, associated with the large igneous province of the CAMP, and is best represented in Iberia by volcano-sedimentary sequences in the Algarve basin (Font et al., 2015) and by the dolerite dike that intrudes the 600 km long Messejana-Plasencia fault (Palencia Ortas et al., 2006; Silva et al., 2008; de Vicente et al., 2021). The CAMP event is also present onshore the study area, as a volcano-sedimentary complex in the Santiago do Cacém basin (**Figure 1**), with basaltic lava flows and tuffs that barely exceed 100 m of thickness (Dias et al., 2016; Inverno et al., 1993).

The second event resulted from melting of metasomatized lithosphere in rifting context at Jurassic-Cretaceous transition age (~145 Ma) (Mata et al., 2015). This event is absent in the study area, occurring as plugs and dikes intruded in rift faults 150 km to the north (to the north of the Nazaré fault).

The third event, known as the West Iberia Alkaline Province (WILCAP) had the longest timespan (onshore from ~94 Ma to 72 Ma (Miranda et al., 2009)) and was the most widespread, with occurrences along the non-rifted basement (Monchique), the rifted margin (Sintra and Sines) and the continent-ocean transition (Madeira-Tore Rise, Gorringe Bank and Guadalquivir Bank) (Merle et al., 2018; Miranda et al., 2009; Neres et al., 2018; Rock, 1982).

The WILCAP is represented onshore in the Lisbon-Sintra region (**Figure 1**) by the plutonic Sintra Magmatic Complex, the Lisbon Volcanic Complex and vast number of dikes and sills (Miranda et al., 2009; Neres et al., 2012, 2014; Terrinha et al., 2017 and references therein). The Sintra magmatic complex consists of two bodies, an older one of gabbro, diorite and syenite and a younger one of granite (75-80 Ma). The oldest WILCAP age of 93.8 ± 3.9 Ma was obtained for the Foz da Fonte dolerite sill (Miranda et al., 2009).

Off Cascais, the high amplitude Cabo Raso magnetic anomaly is known since the XV century because ship compasses deviate from the magnetic North. A dedicated survey by Allan (1965) partly revealed the anomaly shape and associated it to the Sintra intrusive magmatism and the Lisbon volcanism. Apart from low-resolution mapping on later compilations, no further studies have been dedicated to the outstanding Cabo Raso anomaly during decades.

To the south of the Arrábida thrust belt the main known occurrence is the Sines magmatic complex (Ribeiro et al., 2013 and references therein). The onshore Sines complex crops out along an elliptical area of 5x3 km and consists of a central unit of syenite and an external ring of gabbro, with some blocks of gabbro contained within the syenite, with ages 74-78 Ma (Miranda et al., 2009). A multiphase emplacement was inferred from

structural relations (c.f. synthesis in Ribeiro et al 2013). Aeromagnetic data suggested the existence of two magnetic anomalies offshore Sines (Miranda et al., 1989), interpreted together as a large offshore extension of the magmatic complex. Previous work combining magnetic, gravimetric and vintage seismic data estimated an offshore extension of the magmatic complex of 300 km^2 (Carvalho et al., 1998), but this estimation was limited by the low data resolution and large scale of the survey data.

The origin of the WILCAP is still not well understood. It has been attributed to a wide mantle plume or thermal anomaly emitting scattered magmatic pulses during the complex motion of Iberia (Grange et al., 2010; Merle et al., 2006; Miranda et al., 2009), and may be related to a mantle upwelling rising from the seismically slow Central East Atlantic mantle anomaly (Civiero et al., 2021).

Several paleomagnetic and rock magnetic studies have been conducted on outcropping rocks from the WILCAP and CAMP magmatic events (e.g. Barbosa, 1999; Font et al., 2015; Neres et al., 2012, 2014; Ribeiro et al., 2013; Terrinha et al., 2017). Despite these studies focused on different objectives and did not assess the same parameters with the same detail nor statistical significance, the general magnetic character of these rocks can be roughly summarized (excluding samples with secondary magnetic minerals and magnetization). Natural remanent magnetization (NRM) is carried by magnetite or titanomagnetite with values ranging from 10^{-2} to 10 Am^{-1} with most samples within the 0.5 – 3 Am^{-1} interval. Bulk susceptibility varies roughly between 10^{-3} and 10^{-1} SI and Königsberger ratio is usually >1.

3. Methods

3.1. Magnetic anomaly surveying

For this study we acquired, analyzed, and interpreted magnetic data from several magnetic surveys along the Portuguese shelf. Magnetic surveying is a powerful indirect geophysical method for unraveling the subsurface geological structure, often not

recognizable otherwise. The magnetic anomaly field is caused by variations (in both magnitude and direction) of the magnetization distribution $\vec{M}$, according to:

$$\vec{B}(\vec{r}) = -\frac{\mu_0}{4\pi} \nabla_r \int_V \vec{M}(\vec{s}) \,.\, \nabla_s \left(\frac{1}{|\vec{r} - \vec{s}|}\right) dV$$

where $\vec{r}$ is the vector to the observation point and $\vec{s}$ varies within the source volume V (Blakely, 1996). The anomaly field thus depends on the observation point, on the geometry and amplitude of the magnetic sources, and on their interactions. Geological applications study the crustal anomaly field, whose variations can be mainly attributed to changes in magnetization distribution caused by the presence of magnetized bodies (e.g., magmatic intrusions), topography of magnetized layers (e.g., due to tectonics such as tilting, folding and thrusting), and/or contrasts between different lithologies. Significant crustal magnetic anomalies are mainly caused by magnetite-bearing rocks, since a small magnetite content (0.5 wt% of the iron oxide fraction) is enough to dominate the rock magnetic properties (e.g. Tarling & Hrouda, 1993).

The type and dimension of geological structures that can be identified by magnetic data depend both on the resolution (line density and height) of the magnetic survey. **Figure 1c** shows the aeromagnetic map of Iberia, built from Portuguese and Spanish surveys conducted at 3000 m altitude with 10 km line spacing and 40 km tieline spacing (Ardizone et al., 1989; Miranda et al., 1989; Socias & Mezcua, 2002). The large-scale pattern of long-wavelength anomalies is well represented by the aeromagnetic data. However, the higher frequency anomaly field caused by shallower and smaller sources is not detected, and the internal structure of complex anomalies is not resolved (e.g. Oehler & Lequentrec-Lalancette, 2019). For this, high-resolution surveys are needed, in which data are acquired along closely spaced lines.

High-resolution magnetic surveying is also of high value for detection of human artifacts such as ship wrecks or unexploded ordnances (UXOs) and can be mandatory before dragging operations or installation of facilities (e.g. Mil-Homens et al., 2020). In fact, the small-scale geological analysis and interpretation pose additional questions, because it observes a frequency spectrum that overlaps for anomalies of geological and human

origin. This is particularly relevant for the Portuguese coast, where hundreds of archeological artifacts (mainly shipwrecks) exist, many with magnetic signature (Fraga et al., 2015), as well as several submarine cables, outfalls and other man-made structures.

3.2. Seismic interpretation

We complement the magnetic data analysis with interpretation of existing seismic data from the study area. The analyzed profiles include high resolution, low penetration academic seismic data acquired in the scope of research projects (lines MP, TD, PD), and also deep penetration vintage seismic profiles acquired by oil industry exploration surveys (lines GSI). Details on the seismic datasets are given in the Supplementary Text S1, and non-interpreted versions of the profiles are shown as *Supplementary Figures S4 to S12*.

4. Marine magnetic data acquisition

Magnetic datasets were acquired during marine surveys conducted from 2014 to 2019, covering a total surveyed area of ~4400 km^2. *Supplementary Table S1* lists for each survey the dates, number of effective magnetic survey days, research vessel and magnetic base station. **Figure 2** shows the respective acquisition lines.

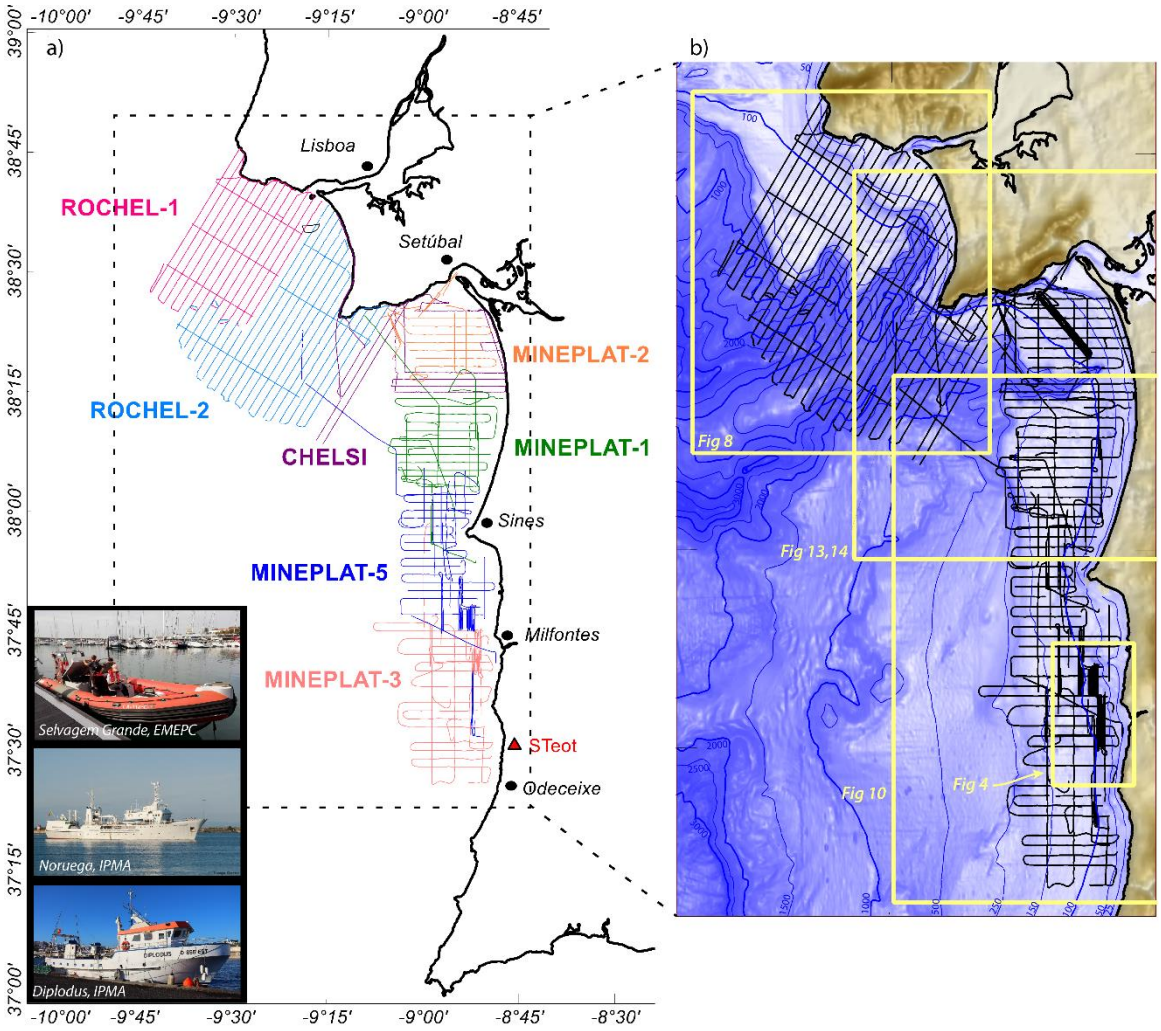

***Figure 2**: **(a)** Survey lines for each magnetic survey. Red triangle locates the IPMA's São Teotónio magnetic base station. Also shown are photos of the research vessels used for acquisition of data used in this work (Supplementary Table S1). **(b)** Location of the areas shown further in this work.*

4.1. The ROCHEL and CHELSI magnetic surveys

The ROCHEL and CHELSI surveys were fully dedicated magnetic surveys conducted onboard Selvagem Grande, a 7.5 m semi-rigid inflatable boat (**Figure 2**, *Supplementary Table S1*). The ROCHEL survey was designed to detail the previously known Cabo Raso magnetic anomaly (Allan, 1965) and to investigate in detail other nearby offshore anomalies, motivated by the fact that very shallow Cretaceous magmatic bodies were

reported by Neres et al. (2014). The CHELSI survey was later designed to fill data gaps between ROCHEL, MINEPLAT-1 and MINEPLAT-2 surveys.

The surveys extended from the Cabo da Roca to south of Cabo Espichel and the western part of the Arrábida thrust belt where Cretaceous dikes and sills crop out (**Figure 2**). ROCHEL covers an area of about 2150 km^2 and more than 1500 km total line length. Survey lines always approached as close as possible to the coastline and extended up to 40 km away from the coast. Deepest surveyed bathymetric levels were ~2500 m across the Lisbon, Cascais and Setúbal canyons. Lines were regularly spaced of 1 nautic mile and tielines were spaced of 5-6 nautic miles. Additional data were acquired during transits and parallel to the coast (over the 10 m isobath).

Total field magnetic data were acquired by a scalar G-882 Cesium marine magnetometer (Geometrics) at 10 Hz logging frequency. Typical surveying ship speed was 10 knots, resulting in along-line resolution of ~0.5 m. The magnetometer was towed with 35 m cable layback, at constant depth about 1 - 2 m below sealevel. GPS positioning was given at 5 Hz by a SIMRAD GS15 GPS antenna, with a 16-channel receiver.

4.2. The MINEPLAT surveys

The MINEPLAT project is a multidisciplinary project searching for mineral resources along the Alentejo inner shelf (Noiva et al., 2017) (https://mineplat.uevora.pt/lizmap/www/index.php/view/map/?repository=mineplat&project=mineplat_geral). The surveys were conducted onboard IPMA's research vessels: the 47.5 m long R/V Noruega and the 17.5 m long R/V Diplodus (**Figure 2**, *Supplementary Table S1*) and were designed for the simultaneous acquisition of ultra-high-resolution multichannel seismics, multibeam bathymetry and backscatter and magnetic data; therefore the magnetic data coverage is not as regular as in ROCHEL and CHELSI surveys. The planned and average line separation was also 1 nautic mile, but some line gaps as well as patches of denser line spacing exist (**Figure 2**). In total, magnetic data were acquired along more than 2300 km line length, covering an area of about 2250 km^2.

Total field magnetic data were acquired by a scalar G-882 Cesium marine magnetometer (Geometrics) at 10 Hz logging frequency. The average surveying speed was ~ 3.5 knots (MCS and MB simultaneous acquisition) or ~6 knots (MB simultaneous acquisition), corresponding to along-line resolution of ~0.2 or 0.3 m, respectively. The magnetometer was towed at sea level with layback of 110 m (R/V Diplodus) or 200 m (R/V Noruega), enough to avoid the interference from the vessel engine and from the UHRS sparker shots. The positioning of the vessel was determined by 2 GNSS antennas complemented by RTK and DGPS corrections and controlled by an integrated system (Applanix POSMV Ocean Master).

5. Magnetic data processing and analysis

Magnetic datasets were processed to combine data from all surveys and achieve a final merged database and final grids for the entire surveyed area.

5.1. Processing of individual surveys

The following processing steps were applied to each individual survey : (i) Layback correction for the magnetometer position using the *Interpolator* algorithm of the MagLog acquisition software; (ii) Spike removal and noise filtering; (iii) Subtraction of the local magnitude of the main Earth's internal field at the time of data acquisition, assuming the International Geomagnetic Reference Field (IGRF) model updated to the survey dates (Thébault et al., 2015); (iv) Correction of diurnal and high frequency variation of the external field using base station data (**Figure 3**, **Figure 4**).

5.1.1. Base station data (external field correction)

Supplementary Table S1 indicates the base station used for each survey, including Coimbra (IAGA code COI) and San Pablo-Toledo (SPT) geomagnetic observatories (data available at 1 minute frequency) and IPMA's São Teotónio base station (raw data at 10 Hz acquisition frequency, operating since 2016). Base station data were processed and applied as follows: down-sampling to 1 minute frequency (São Teotónio data); low-pass filtering for 20 minutes cut-off wavelength, to avoid local high frequency fluctuations; calculation of the local diurnal anomaly by subtraction of a baseline value; correction of survey data (**Figure 3**). **Figure 4** illustrates the effect of base station correction for a part of Mineplat-3 area. The strong artifact effect of line paths in the uncorrected data grid (**Figure 4c**) is removed after applying base station correction (**Figure 4d**). Base station correction showed to be very effective for all surveys, supporting that each respective recording of external field variations could be accurately assumed for the surveyed area. This correction was particularly well succeeded for the surveys corrected with IPMA's São Teotónio observatory data. ROCHEL surveys, corrected with the 200 km far

Coimbra base station data (São Teotónio was still not operating), showed the less accurate improvement.

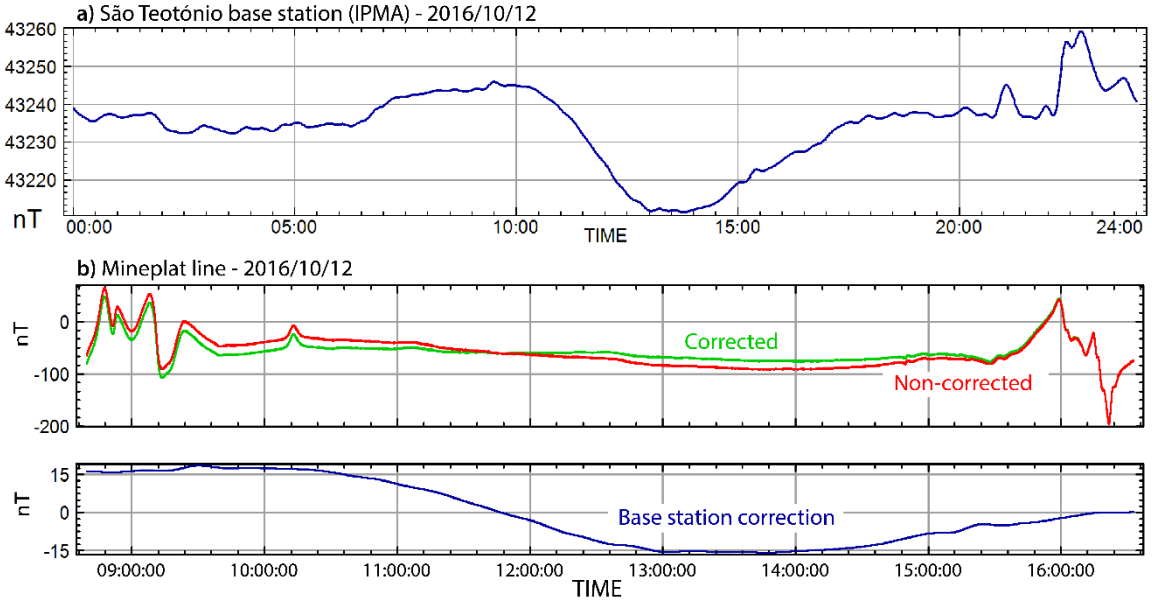

***Figure 3**: **(a)** 24h record of total magnetic field in the São Teotónio base station, and **(b)** respective use for correction of a MINEPLAT acquisition line.*

5.2. Merging of surveys

Corrected data from all surveys were merged into a single database, simultaneously leveled, and gridded. Leveling was iterative (3 iterations) and assumed a zero-order trend for each individual line. The linear trend is preferred to higher order fits because after accurate base station correction no significant high frequency variations are expected within lines; on the contrary, if allowed, non-linear trends could input spurious unrealistic anomalies in the data. Line leveling decreased the cross-line intersection standard deviation in 37%, from 5.5 nT to 3.5 nT. **Figure 4e** shows the final leveled grid for the Milfontes area. All grids were produced for 100 m cell size using minimum curvature interpolation. The final magnetic anomaly grid is shown in **Figure 5a**.

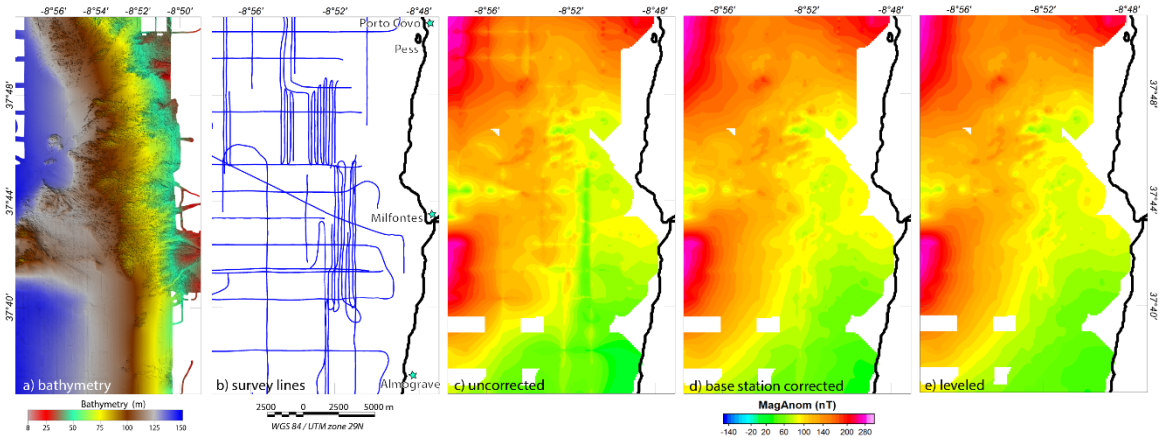

Figure 4: *Illustration of corrections applied during magnetic data processing, for a detail of Mineplat-3 area off Vila Nova de Milfontes, which includes patches of denser magnetic sampling.* ***(a)*** *Survey lines of magnetic data acquisition.* ***(b)*** *Full coverage multibeam bathymetry acquired during Mineplat surveys, processed.* ***(c)*** *Uncorrected magnetic anomaly gridded data.* ***(d)*** *Magnetic anomaly after applying base station correction (São Teotónio observatory, STT).* ***(e)*** *Magnetic anomaly after iterative line leveling. Base station correction and line leveling greatly improved data consistency and allow confirming the existence and continuity of anomalies. Pess: Pessegueiro Island. For location see* ***Figure 2****.*

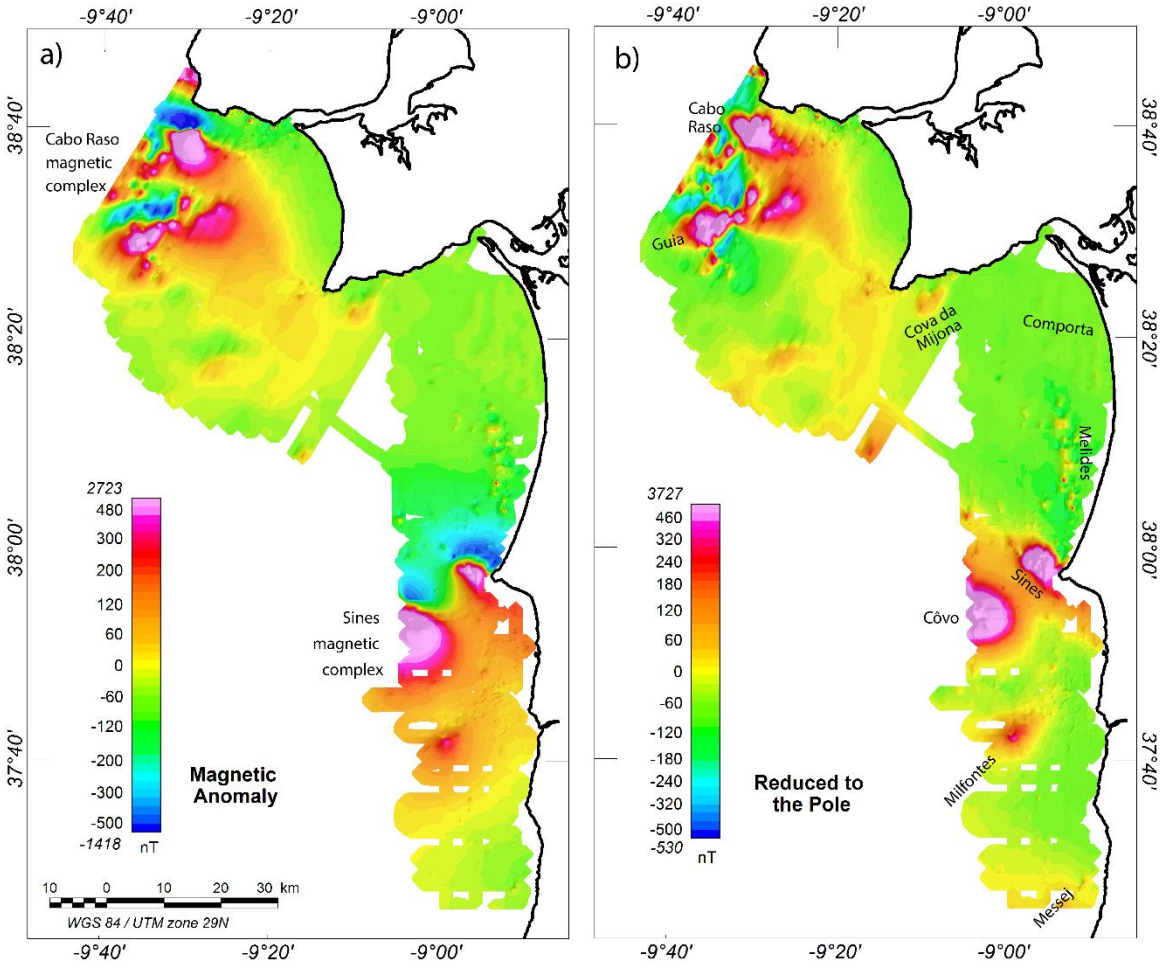

Figure 5: *Observed magnetic anomaly field (sea-level).* ***(a)*** *Final magnetic anomaly field after complete data processing. The Cabo Raso and Sines magnetic complexes are identified.* ***(b)*** *Reduced to the pole magnetic anomaly, and labeled magnetic anomalies discussed in this work. Italic labels in the color scales correspond to maximum and minimum grid values that are not resolved in the saturated color scale.*

5.3. Potential field transformations

Potential field transformations (upward continuation, reduction to the pole and derivative fields) were applied to the processed data to assist interpretation of the magnetic anomalies, providing insights into the nature and location of the sources (Blakely, 1996).

Upward continuation calculates the field as if it was measured at a different height. It acts as a low-pass filter, accentuating anomalies caused by deep sources and attenuating shorter wavelength shallow sources, including noise. Upward continuation was calculated for 600 m and 3000 m heights (**Figure 6a,c**), which correspond to the flight altitudes of aeromagnetic surveys conducted for Portugal and Spain (3000 m) (Socias & Mezcua, 2002), and for the Portuguese margin (600 m; industry offshore surveys). The 200 m upward continued field is also presented in *Supplementary Figure S1a*.

Reduction to the pole transformation (RTP) shifts the anomalies to be located over respective bodies and changes their shape compensating for the skewness effect due to the non-verticality of the ambient field and magnetization vectors. The anomaly field, as well as the upward continued fields were reduced to the pole (RTP) considering IGRF inducing field parameters (inclination 52°; declination -3°) (Thébault et al., 2015) (**Figure 5b**; **Figure 6b,d;** *Supplementary Figure S1b*). RTP assumes that the magnetic anomaly is mainly due to induced magnetization, disregarding eventual remanence of the source bodies.

Derivative fields are helpful in defining anomalies that may not be evident in the total anomaly field, and in discriminating different types of anomalies / source bodies (Blakely, 1996).

Horizontal gradient magnitude: $\frac{\partial A}{\partial h} = HD = \left[\left(\frac{\partial A}{\partial x}\right)^2 + \left(\frac{\partial A}{\partial y}\right)^2\right]^{1/2}$

Vertical derivative: $VD = \frac{\partial A}{\partial z}$

Tilt derivative angle: $TD = \arctan\left(\frac{VD}{HD}\right), \in \left[-\frac{\pi}{2}, \frac{\pi}{2}\right]$

Analytic signal amplitude: $as = \left[\left(\frac{\partial A}{\partial x}\right)^2 + \left(\frac{\partial A}{\partial y}\right)^2 + \left(\frac{\partial A}{\partial z}\right)^2\right]^{1/2}$.

The magnitude of the horizontal gradient (here horizontal derivative) has maxima located over the edges of the sources and is particularly effective in locating abrupt lateral changes in magnetization across vertical edges. The vertical derivative enhances and resolves shallow sources (short-wavelength field components). The tilt derivative, or tilt angle, enhances low amplitude anomalies because it is independent from the anomaly amplitude. The analytic signal amplitude, or total gradient, has maxima over the magnetic sources. It is independent from the magnetization of the source bodies and does not need previous RTP (Nabighian, 1972) This is especially useful when the source bodies carry a significant remanence, which is typically the case for magmatic rocks with significant thermoremanent magnetization. Derivative calculations in the Fourier domain (fft) used a distance increment of 100 m, which was found to be a good compromise between attenuation of high-frequency noise and retaining of the significant spectrum of anomalies.

Figure 7 presents the horizontal, vertical and tilt derivatives calculated for the RTP 600 m upward-continued field, and the analytic signal calculated of the 600 m upward continued field.

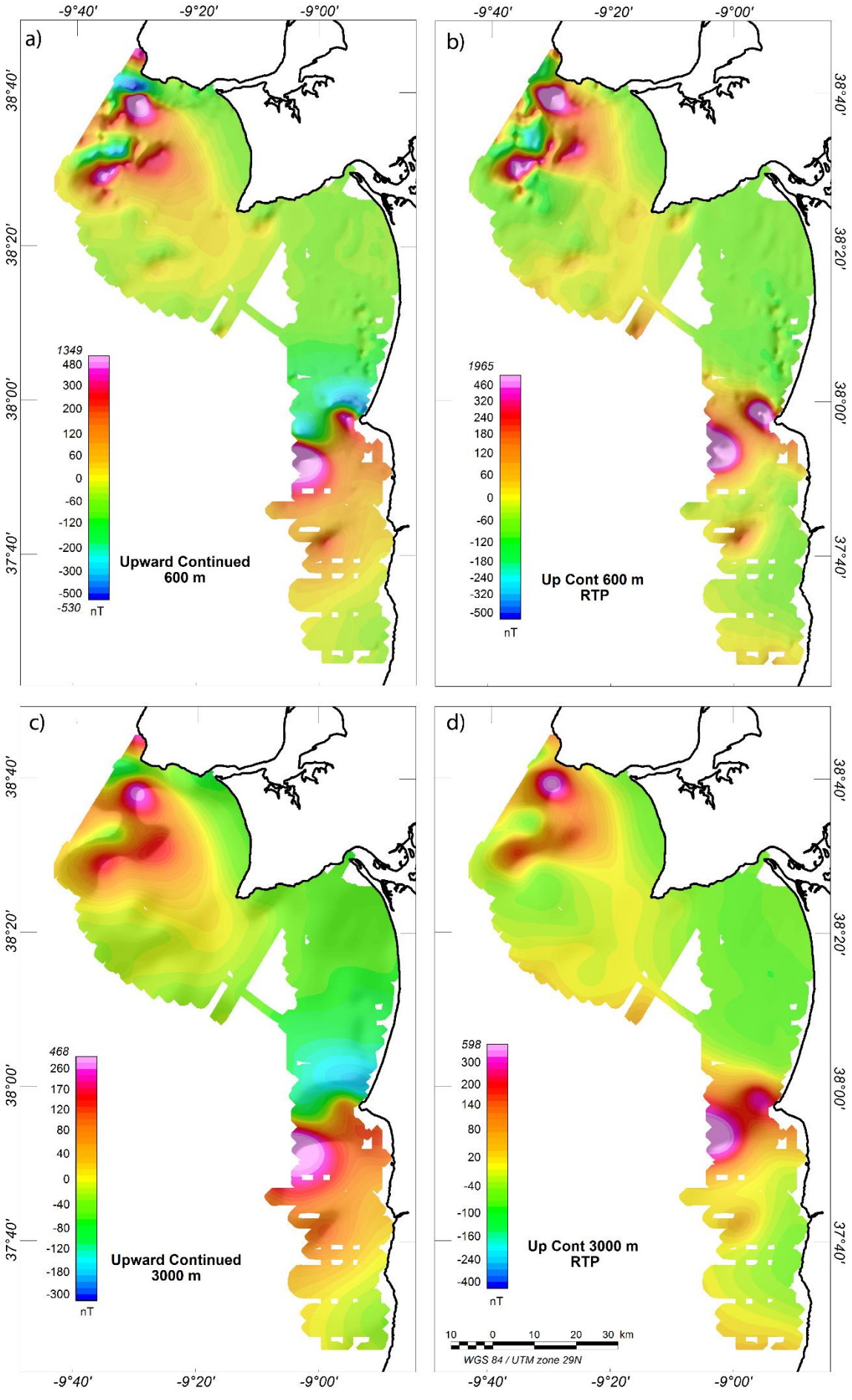

Figure 6: ***(a)*** *Magnetic anomaly field upward continued to 600 m and* ***(b)*** *its reduction to the pole (RTP).* ***(c)*** *Magnetic anomaly field upward continued to 3000 m and* ***(d)*** *its reduction to the pole (RTP). 3000 m was the flight altitude of aeromagnetic surveys conducted for Portugal and Spain (Ardizone et al., 1989; Miranda et al., 1989), thus c) can directly be compared to* ***Figure 1****d and interpreted as its offshore prolongation, except that our marine survey was conducted with much higher line density (i.e., resolution) and therefore some of the anomalies would not be sampled by the sparser flight lines. The high frequency content related to shallower sources is strongly attenuated and the low frequency field caused by deep sources remains as blurrier anomalies.*

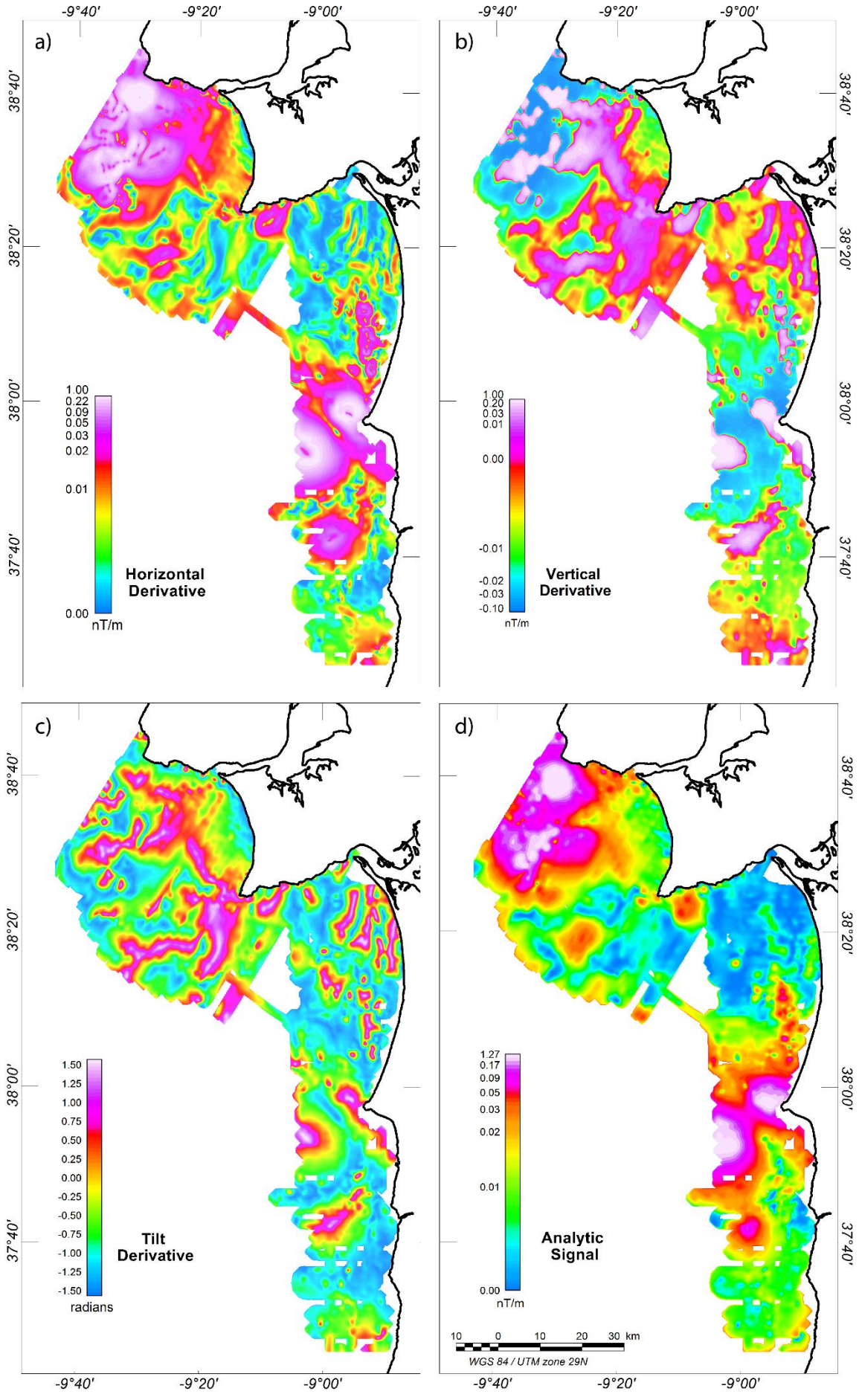

Figure 7: *Derivative fields:* ***(a)*** *magnitude of the horizontal gradient;* ***(b)*** *vertical derivative;* ***(c)*** *tilt derivative;* ***(d)*** *analytic signal. The derivatives were calculated for the 600 m upward continued anomaly grid to avoid high-frequency noise. Potential field transformations reveal different aspects of the magnetic anomaly field spectrum. The analytic signal is maximum over the main magnetic sources, whereas the horizontal derivative is maximum over their limits, especially if abrupt vertical edges. The vertical and tilt derivatives enhance the short wavelength anomalies, but the tilt derivative has the further advantage of similarly detecting low and high amplitude anomalies. E.g., the low amplitude Comporta lineations, the Roca-Espichel fault / dike, the Melides alignment of anomalies, the strike of the high-frequency component of the Milfontes anomaly (see* ***Figure 5****b for location) are best identified through derivative fields.*

Given the large variety of anomalies it was essential to conduct thorough analyses of both along-line data and gridded calculated fields for correlating and characterizing the anomalies. Tilt and vertical derivatives were useful for verifying the across-line correlation of short-wavelength and/or low-amplitude lineations, overcoming the limitation on resolution imposed by the line spacing to confirm the spatial continuity of anomalies. Filtering of anomalies using high- and low-pass filters (10 km cutoff wavelength) was also used to isolate the short and long-wavelength components of the field. This was especially helpful for the Tagus Delta area (Figure 8**b**).

Despite the improvement achieved through line correction and leveling (**Figure 4**), some residual unleveling still remains as high frequency noise in the anomaly grid. This noise is enhanced in the frequency-domain-calculated RTP (**Figure 5**b) and affects especially the ROCHEL surveys. We do not filter this noise because it would eliminate real short-wavelength anomalies. We rather evaluate the real versus artifact character of the anomalies whenever necessary by analyzing in detail the along-line data and the derivative and upward continued fields.

6. Results and interpretation of magnetic zones

The observed magnetic anomaly field (**Figure 5**) has a wide spectrum of anomalies, with amplitude varying from < 20 nT to > 4100 nT (peak-to-peak) and wavelength from ~500 m to >10 km. The more significant anomalies in amplitude and size concentrate in two zones, Cabo Raso and Sines that are characterized by large, long-wavelength anomalies superimposed by other scattered shorter anomalies, potentially indicating the coexistence of deep large sources with smaller-scale, punctual or planar shallower sources, and/or a possible interplay of remanent and induced magnetization. Because of their size and complexity, we named these zones the Cabo Raso and the Sines magnetic complexes. We next describe them in detail, as well as other magnetic anomaly zones.

6.1. The Cabo Raso magnetic complex and the Roca-Espichel anomaly zone

The ROCHEL survey data reveals with unprecedented detail a complex anomaly field with wide amplitude and wavenumber spectra (**Figure 5**; Figure 8). The highest and widest anomalies concentrate over the continental shelf (< 200 m bsl), where a high density of both long and short wavelength anomalies of very high amplitude is observed (Figure 8a**,b**), the Cabo Raso magnetic complex. Many high amplitude (> 500 nT) anomalies with variable wavelengths indicate the presence of several highly magnetized bodies, i.e., magmatic rocks of various sizes emplaced at different depths.

The Cabo Raso anomaly is the most outstanding, with ~7 km wavelength, > 4100 nT amplitude (L1 in Figure 8), very high horizontal gradients (up to 5 nT/m) and analytic signal (**Figure 7**). This indicates the presence of a highly magnetized vertical-edged, deep-rooted plug-like volcanic body. Its short-wavelength (shallow) component strikes parallel and within the 50 m and 100 m isobaths (Figure 8**b**). Nearby shorter anomalies suggest the existence of several smaller intrusions.

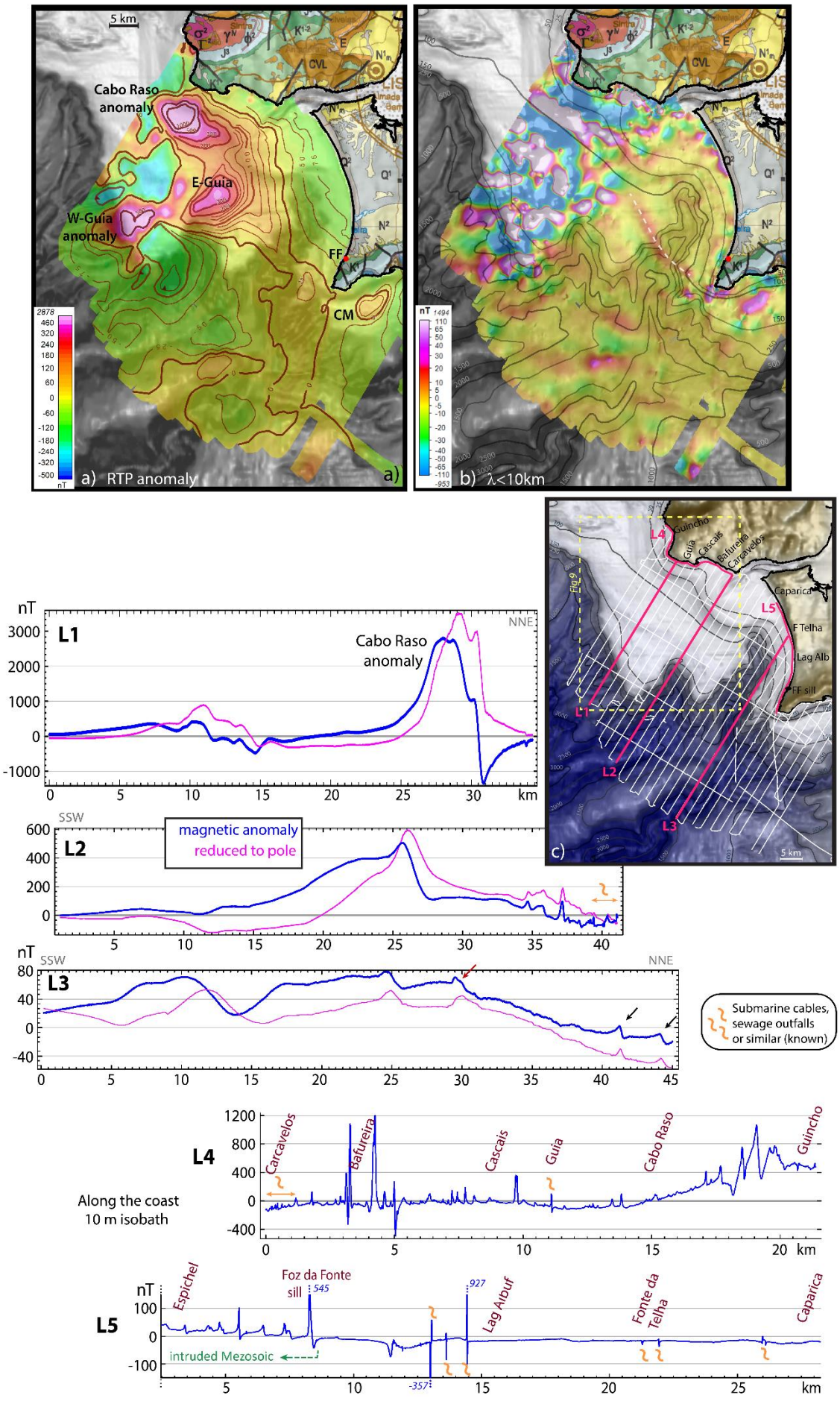

*Figure 8: The Cabo Raso magnetic complex and the Roca-Espichel anomaly zone (**Figure 2** for location). **(a)** RTP magnetic anomaly and respective contour lines, over a bathymetric background. Countour lines are plotted for multiples of 25 nT (thin lines), 100 nT and 500 nT (suppressed when high line density). CM: Cova da Mijona anomaly; FF: Foz da Fonte sill.*
***(b)** Short-wavelength anomaly field (anomaly filtered to wavelengths < 10 km). Contour lines are isobaths (25, 50, 100, 150, 250, 500, 1000, 1500, 2500, 3000 m). The white dashed line marks the linear NW-SE anomaly (also evident in **Figure 7**) that may correspond to the Roca-Espichel fault zone. Note that this anomaly coincides with the deflection of the bathymetric contours, on each side of the Lisbon canyon (cf. Figure 1a).*
***(c)** Bathymetric map and survey lines. Highlighted are L1-L5 lines, for which we show the along-line magnetic anomaly. Note that the ordinate scales vary for each line, and that for L5 it is truncated – maximum and minimum values for larger anomalies are written in italic blue. The abscissa scale is maintained among L1-L3 and among L4-L5.*
*L4 and L5 were surveyed over the 10 m isobath (constant altitude) along the Carcavelos – Guincho and Cabo Espichel – Costa da Caparica coastlines, respectively. Yellow marks indicate anomalies that coincide with mapped submarine cables, sewage outfalls or similar human structures (https://geomar.hidrografico.pt/). Several anomalies of several hundred nT are observed along the whole length of L4 and are attributed to the presence of small-scale magmatic bodies, most likely dikes. Along L5, the 94 Ma Foz da Fonte sill (FF; 587 nT peak-to-peak, red circle in b) marks the transition between a "non-magnetic" domain (towards the north up to Caparica), and a southern domain (from FF to Espichel Cape), where several anomalies up to 100 nT are observed. Black arrows in L3 mark anomalies that form the N65°W lineations observed in **Figure 7**b, and the red arrow shows the intersection with the Roca-Espichel lineation.*

The Guia anomaly (Figure 8)**,** is a N75°E-elongated, 30 km long and 7 km wide anomaly (>1500 nT peak-to-peak) that comprises long and short wavelength components, suggesting the association of shallower magmatic plugs with a deeper intrusion.

The Cabo Raso magnetic complex lies within a highly intruded zone of magmatic bodies in the SW of the Lusitanian Basin (***Figure* 1**). Towards the deep offshore, the Cabo Raso magnetic complex is limited by the shelf break slope (Figure 8). Its eastern limit appears to be related to the Cascais and Lisboa canyons. The high frequency anomaly zone

(Figure 8**b**) abuts the prolongation of the Cascais canyon towards the onshore NE-SW fault (**Figure 1**b).

To the east of the highly intruded zone the anomaly amplitude decreases, reaching negative values towards the coast. Nonetheless, some low amplitude lineations stand out from this negative anomaly zone. The most significant is a ~20 km long NNW lineation (highlighted as a white dashed line in Figure 8b and also evident in **Figure 7** derivative fields) that runs from the E-Guia anomaly zone towards Cabo Espichel. This anomaly shows 20-40 nT amplitude, and suggests the presence of a dike coincident with the Roca-Espichel fault zone proposed by (Terrinha et al., 2017). Other lineations of ~10 nT amplitude run from the coast striking N65°W, as observed mainly in the vertical derivative grid (**Figure 7**b) and along-line profiles (Figure 8, black arrows in L3).

From the Foz da Fonte sill (600 nT anomaly) towards Cabo Espichel a positive gradient is observed, superimposed by several high-frequency anomalies (L5 in Figure 8; cf. Section 6.1.3). To the south of the Arrábida chain a 5km, >110 nT anomaly stands out (Cova da Mijona anomaly) (cf. Section 6.4). This anomaly is most likely due to the presence of magmatic intrusion deforming the Mesozoic rocks as proposed by (Kullberg et al., 2000; Vinhas da Costa, 2018). It is worth noting that this anomaly is on the prolongation of an onshore tectonic inversion structure that accommodated the extrusion of the Sesimbra shale and gypsum wall, which is intruded by a series of alkaline basic dikes (Figure 14).

The NW-SE striking Roca-Espichel dike locally deflects the bathymetry contours on both flanks of the Lisbon canyon, an indication of its very shallow position. This is possibly a magma conduit connecting the Cabo Raso magmatic intrusions with the smaller magmatic complex of Foz da Fonte, Cova da Mijona intrusion and Sesimbra sills, exposed due to the exhumation of the Mesozoic formations along the Arrábida thrust belt. The existence of such a magmatic conduit was postulated by Neres et al. (2014), connecting the Foz da Fonte sill through the Cabo Raso, the Fontanelas volcano in the Estremadura Spur to the Madeira-Tore Rise volcanic ridge, i.e. a magmatic lineament of >350 km of length.

6.1.1. Seismic imaging of the Cabo Raso intrusion

The Cabo Raso anomaly has been related to the presence of an intrusion imaged by seismic data (Neres et al., 2014). Figure 9 shows the Cabo Raso intrusion along two recently acquired seismic reflection profiles. This forced intrusion (U2) cuts through Lower Cretaceous sediments (unit U1) that are unconformably overlain by undeformed post-Miocene sediments (U3). The intrusion is covered by seismic Unit U4, coeval with the Tagus River submarine delta of post-Last Glacial Maximum age (Terrinha et al., 2019b). The Cabo Raso intrusion coincides with the maximum observed analytic signal (Figure 9) which assigns it to the shallowest crest of the magnetic source. However, the very high amplitude and gradients and the km-scale of the anomaly claim for the presence of a deep-rooted plug-like magmatic intrusion as this shallow imaged source is insufficient to justify the observed anomaly. Considering that U2 is ~5km long on the shallow profile PM30 (Figure 9) it compares in size with the outcropping Sintra plutonic intrusion that is roughly 6 km along the N-S direction (**Figure 1**).

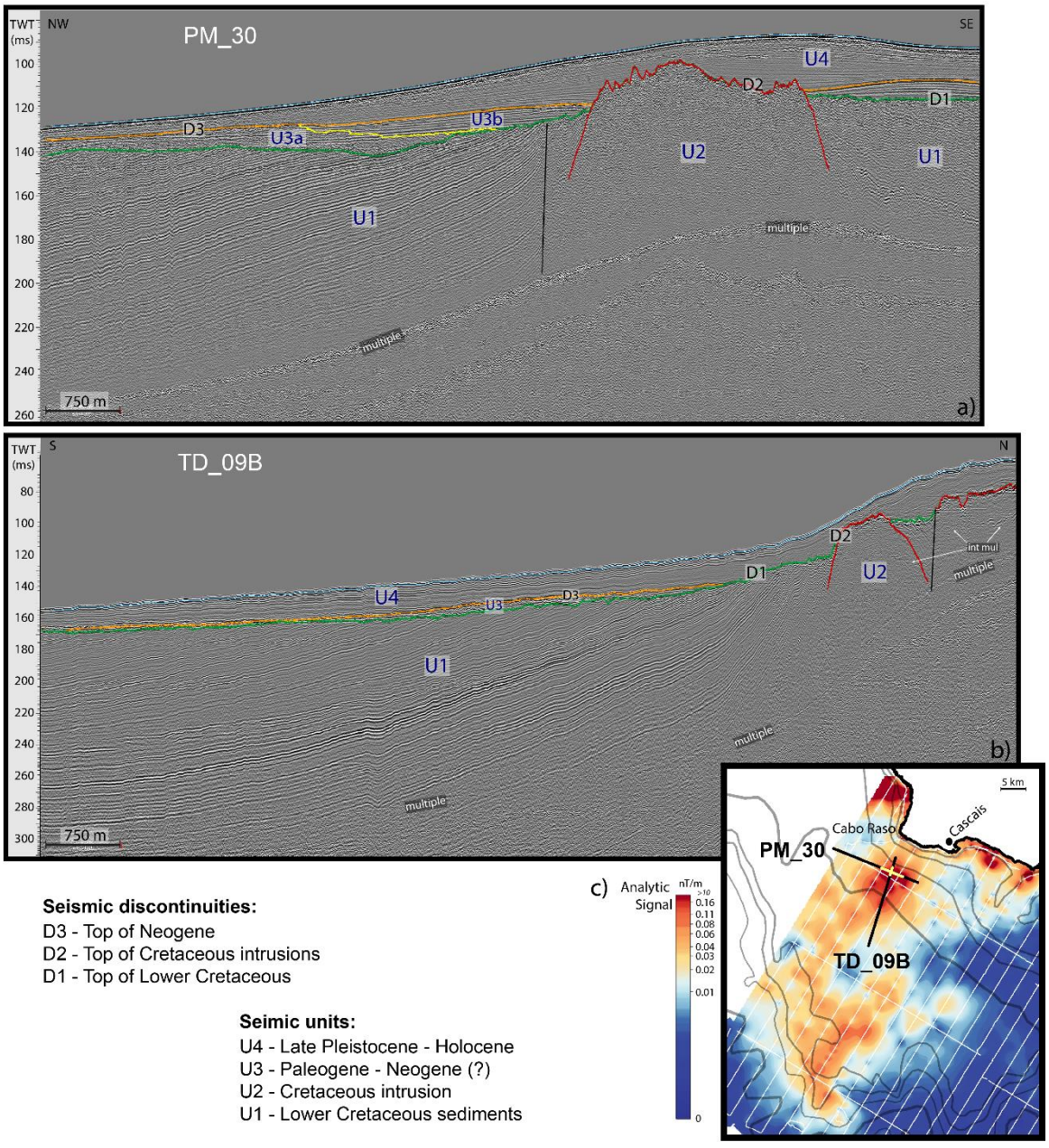

Figure 9: Seismic profiles across the Cabo Raso magnetic anomaly. ***(a,b)*** *The body marked as seismic unit U2 forced its intrusion into the Cretaceous of the Lusitanian rift Basin (U1) in a similar process as the Sintra igneous pluton. Seismic units U3 correspond to post-exhumation of the Cabo Raso intrusion, possibly of Paleogene-Neogene age. Seismic unit U4 covers the Cabo Raso intrusion with 8 m of clastic sediments and corresponds to the distal part of the Tagus ebb delta (pro-delta) (Terrinha et al., 2019b).* ***(c)*** *Map (located as yellow rectangle in Figure 8c) locating the two seismic profiles on top of the analytic signal calculated along line (c.f. Section 5.3). The intrusive body U2 (yellow segment on top of each line) coincides exactly with the analytic signal maximum, supporting that it is the topmost part of a deep magmatic source. Int mul: internal multiple ("peg leg").*

6.1.2. Geological versus human origin of the anomalies (artifacts)

The interpretation of ROCHEL magnetic data is not straightforward due to the coexistence of geological and anthropic anomalies. To support the geological interpretation, we cross-analyzed our results against information on the location of anthropogenic structures. Anomalies due to shipwrecks are very localized and irrelevant to the scale of our analysis. The location of submarine cables and other significant structures was taken from navigation maps available at https://geomar.hidrografico.pt/ and checked against the along-line observed data to detect their eventual signature in our data. Cable manholes located at Carcavelos, Caparica and Fonte da Telha, as well as sewage outfalls at Guia (west of Cascais) and south of the Lagoa de Albufeira, correspond to observed magnetic anomalies on lines very close to the coast (at 10 m water depths only, with the magnetometer being towed at average 2 to 3 m of depth. These anomalies are pointed out with yellow signs on L2, L4 and L5 (Figure 8). They are consistently very short wavelength (10-30 m) and their amplitudes vary from tens to 1000 nT (Figure 8). Their signature was not detected or is negligible in survey lines farther from the coast, i.e., it rapidly vanishes with depth.

6.1.3. Surveys along the coast (over the 10 m isobath)

To understand the variability of the anomaly field for fixed acquisition conditions (constant height above seafloor) two lines were surveyed on top of the 10 m isobath along the coast (L4 and L5 in Figure 8).

The Carcavelos – Guincho coast (L4) shows a high density of high-frequency anomalies with typical >100 nT amplitude. The highest anomalies are in the Bafureira-Parede region. Along this coast, dozens of volcanic dikes crop out on the beaches and are thus related to many of the observed anomalies. From Cabo Raso northwards, the anomaly shows a long wavelength increase as approaching the Sintra pluton. Several anomalies offshore Carcavelos and one anomaly west of Cascais are attributed to submarine network cables and to the Guia sewage outfall, respectively.

Along the Caparica – Espichel coastline (L5) two domains can be distinguished: a northern "non-magnetic" domain where almost all the significant anomalies can be assigned to mapped submarine cables or similar manmade structures; and a southern domain where a larger density of anomalies up to 100 nT are observed. The distinct magnetic signature of these two domains is attributed to the contrast between the Cenozoic and Mesozoic stratigraphic record, namely to the presence of Upper Cretaceous dikes and sills as magnetic sources. The boundary between the Cenozoic and Mesozoic formations is outlined by the 8 m thick micro-gabbro Upper Cretaceous Foz da Fonte sill, hosted in Lower Cretaceous sediments that causes a ~600 nT anomaly.

6.2. The Sines magnetic complex

The MINEPLAT data resolve with detail the magnetic anomaly field offshore Sines and along the shelf, confirming that it comprises two distinct main anomalies, here called the Sines and Côvo anomalies (**Figure 10**).

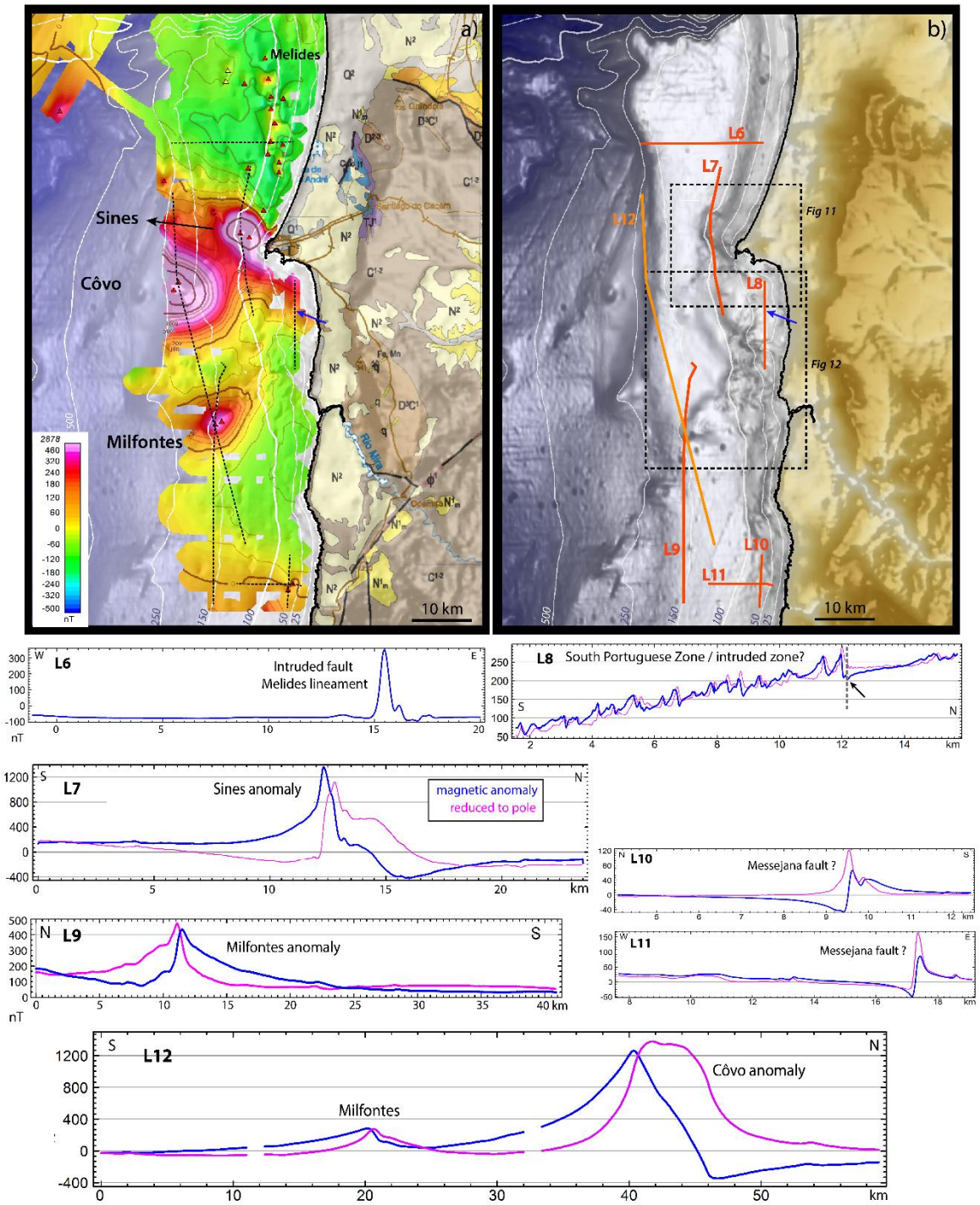

Figure 10: *Magnetic mapping of the Alentejo shelf, including the Sines magmatic complex and the Melides magnetic lineament. Refer to* ***Figure 2*** *for location.* ***(a)*** *RTP magnetic anomaly and respective contour lines, plotted for multiples of 25 nT (thin lines), 100 nT and 500 nT (suppressed when high line density). Triangles locate anomaly local maxima (red: > 100 nT; yellow: < 100nT). White contours are isobaths (same as in b). Onland: 1:10^6 geological map (LNEG), shadowed by topography. Three anomalies outstand in both amplitude and extension: Côvo (L12), Sines (L7;* ***Figure 11****) and Milfontes (L9; Figure 12). Also outstanding is the 20 km long, ~N-S lineament of isolated magnetic anomalies forming the Melides magnetic lineament*

*(**Figure 13**, Figure 14). The Côvo anomaly is only partially surveyed, however its high amplitude, wide extension and lack of bathymetric expression indicates the presence of a deeply-intruded, large and highly magnetized body.*

***(b)** Bathymetric-topographic map with location of profile lines shown below.*

***L6-L12 –** Along-line data (corrected magnetic anomaly and calculated RTP) for selected survey lines (except L12 that was sampled from gridded data). Note that both ordinate and abcissa scales vary for each line. The arrow on L8 (maps and profile) marks the northern limit of a high-frequency anomaly zone that also likely aligns with the southern border of the Sines anomaly.*

6.2.1. Sines anomaly

The offshore Sines magnetic anomaly extends along the NW-SE direction for >10 km with 5 km width (**Figure 10**a), lying on the continuation of the onshore Sines magmatic complex. The anomaly amplitude reaches 1800 nT amplitude (peak-to-peak) (**Figure 10**, **L7**) and comprises a longer-wavelength component (~5 km wide) and a shorter (< 1 km wide) high-amplitude anomalies. Horizontal gradients are very high, up to 3.5 nT/m, particularly for the southern branch of the RTP anomaly. Local maxima of >100 nT also align along the NW-SE direction (triangles in **Figure 10**a). This magnetic anomaly is compatible with the existence of a NW-SE trending magmatic source extending from the onshore outcropping complex, bounded at south by a sharp vertical limit. The Sines magmatic complex intruded along the stratigraphic limit between the Paleozoic and Mesozoic sequences, parallel to the NW-SE trend of the Paleozoic orogenic fabric.

The joint analysis of magnetic data with multibeam bathymetry (**Figure 11**a,b) allowed for outlining the limits of the Sines magmatic complex and its contact with the hosting rocks. The coincidence of magnetic and bathymetric features is clear. A concentric bathymetric pattern is centered in the magnetic anomaly zone, reflecting a near-vertical concentric contact between the host rock and the magmatic intrusive body.

Field inspection along the coast south of the magmatic complex confirms a vertical contact with Paleozoic formations. At north, the contact between the gabbro and the Jurassic limestones of the Alentejo rift Basin is also vertical and comprises a ~85 m thick basaltic sill hosted in the Jurassic rocks (**Figure 11**d). The gabbro contains an intrusion of

syenite, whose dikes cut across both the gabbro and the Jurassic limestones. All these Mesozoic formations are covered by the Quaternary sands and Miocene-Pliocene sandstones.

This combined analysis allowed improving the geological mapping of the offshore outcropping and sub-cropping units, namely the Sines magmatic complex and its host units, the Jurassic sediments: the South Portuguese Zone flysch sequence and the Cercal volcanic-silicious complex (**Figure 11**c). The coordinates of the polygons that delimit the magmatic complex and Jurassic sediments areas are provided as Files S1 and S2, respectively.

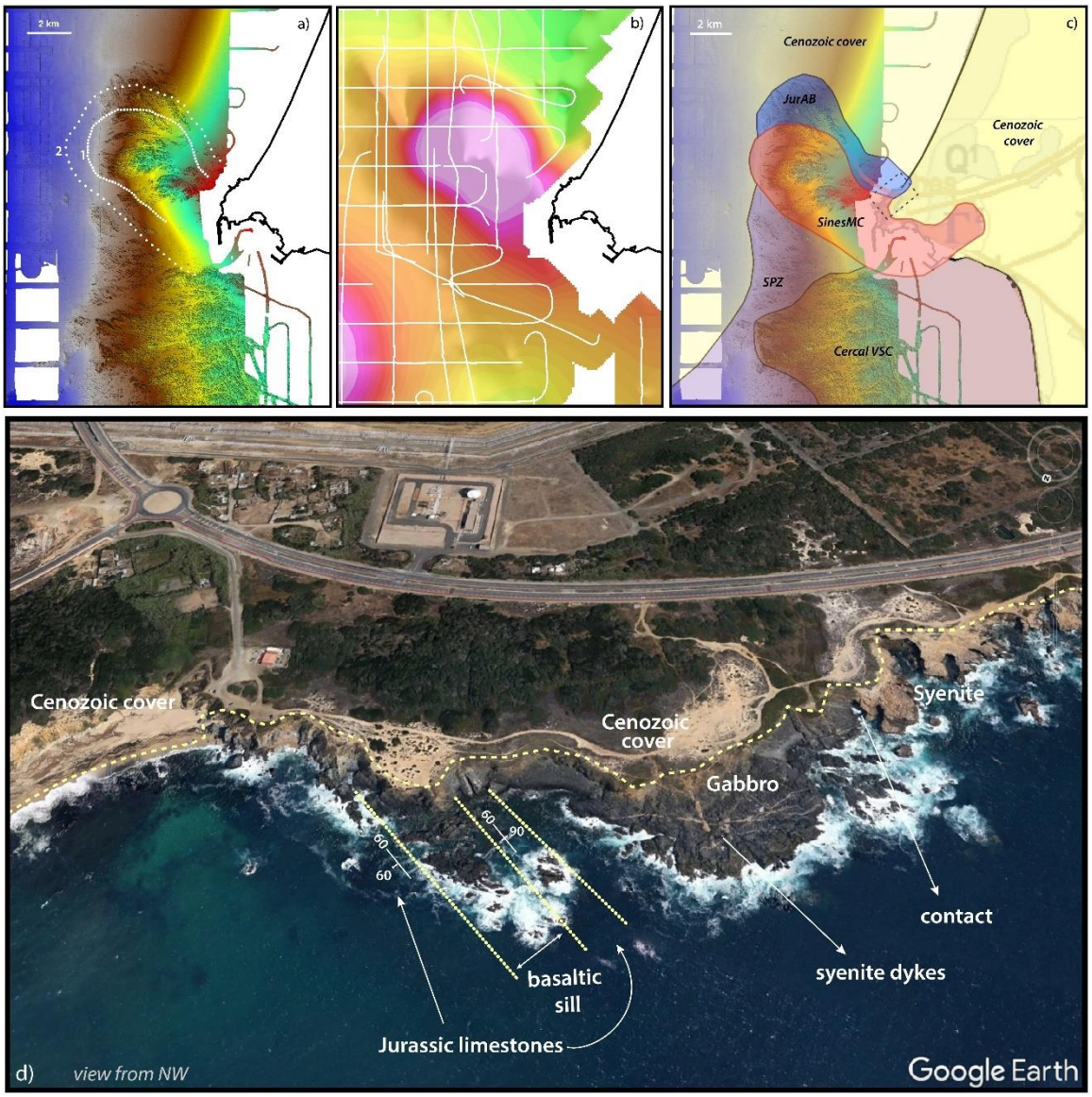

Figure 11*: Sines magmatic complex, limits and surrounding units.* ***(a)*** *Full coverage multibeam bathymetry acquired by IPMA for MINEPLAT project offshore Sines. Location in* ***Figure 10****. White dashed lines (1 and 2) are defined from magnetic data analysis: 1 (internal limit): maximum of horizontal derivative that indicates most abrupt changes over near-vertical body edges; 2 (external limit): 200 nT isocontour of magnetic anomaly / outline for high tilt and vertical derivatives.* ***(b)*** *Coincident RTP magnetic anomaly with overlaid survey profiles. The Sines anomaly is the prolongation towards NW of the onshore magmatic complex (cf. (Ribeiro et al., 2013) for magnetic properties of Sines magmatic rocks). The limit of the anomaly parallels a close-to-vertical foliation that is due to the deformation induced in the host rock by the magmatic emplacement.* ***(c)*** *Geological mapping of outcropping and subcropping units based on magnetic and bathymetric analysis and on field work along the coastline. SinesMC: Sines magmatic complex; JurAB: Jurassic sediments of the Alentejo rift Basin, intruded by sills and dikes; SPZ: South Portuguese Zone flysch sequence (Carboniferous); Cercal VSC: Cercal volcanic-silicious complex (Devonian). The coordinates for the SinesMC and JurAB polygons are provided as Supplementary Files S1 and S2, respectively.* ***(d)*** *Perspective photo (viewed from NW) of the northern outcrop of the magmatic complex and its contact with the host rocks This area is located in (b) as a dashed gray rectangle,.*

6.2.2. Côvo anomaly

The Côvo magnetic anomaly was not completely surveyed by the MINEPLAT project that aimed at mapping the continental shelf only. It shows maximum ~1600 nT amplitude (peak-to-peak) and ~10 km wavelength along N-S direction (**Figure 10**, L12). Compared to Sines anomaly, Côvo has a similar magnetic anomaly amplitude and a larger wavelength, but does not deflect the bathymetry contours or the Paleozoic fabric in the surveyed area (**Figure 10**a,b; **Figure 11**a). This implies that the Côvo anomaly is caused by a buried magnetic source with significantly higher total magnetization than the Sines source body either due to a larger volume of magmatic material and/or to a higher content in magnetite.

6.2.3. Milfontes anomaly

The Milfontes anomaly, found 30 km to the south of Sines, is revealed for the first time. It shows 360 nT maximum observed amplitude and elongation parallel to the NE-SW direction (**Figure 10**, L9, L12; Figure 12). The joint analysis of magnetic data, multibeam bathymetry, ultra-high-resolution and deep multichannel seismic profiles (Figure 12) shows that the Milfontes anomaly coincides with a NE-SW striking fault-bounded Paleozoic basement high. The NW flank is downthrown and there is no evidence for extrusive or exhumed magmatic bodies, which claims for the existence of a plutonic buried source.

Several minor NE-SW trending anomalies were mapped extending for approximately 20 km northeastwards of the Milfontes anomaly (**Figure 4**; **Figure 10**, L8), parallel to its elongation direction. With up to 60 nT amplitude and 300-500 m wavelength, these anomalies depict a confined high-frequency anomaly zone (L8 of **Figure 10**, Figure 12b). They may be due to a horse-tail pattern of dike-like intrusions originated at the Milfontes main anomaly body that profited from the existence of the NE-SW fault system.

About 30 km to the south of the Milfontes anomaly zone, in the southern limit of the surveyed area, a 0.5 km wavelength and 130 nT amplitude anomaly was surveyed in two lines indicating a sharp NE-SW oriented anomaly that corresponds to the orientation of the onshore Messejana fault (**Figure 10**, **L10, L11**), about 5 km north of its prolongation towards the coastline.

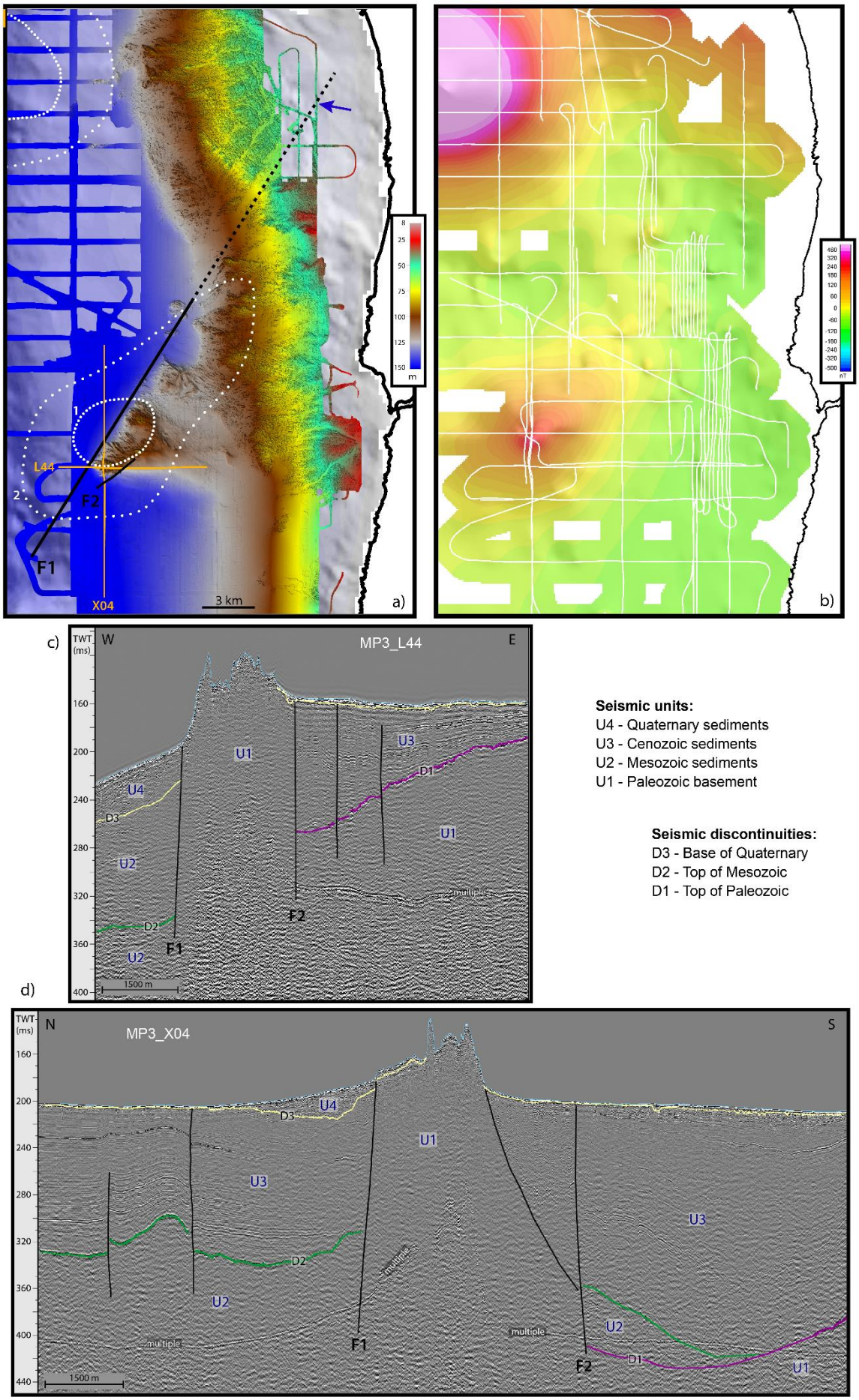

Figure 12: Milfontes anomaly. ***(a)*** *MINEPLAT multibeam bathymetry of the Milfontes magnetic anomaly zone. Location in* ***Figure 10****. Note i) the limit of the rock outcrop that corresponds to steep fault; ii) the NW-SE trending Paleozoic metamorphic foliation south of the fault; iii) the NE-SW trending lineaments (post-foliation fractures). White dashed lines (1 and 2) are defined from magnetic data analysis: 1 (internal limit): horizontal derivative maximum; 2 (external limit): outline for high tilt and vertical derivatives (also shown for the Côvo anomaly at the top left corner).* ***(b)*** *Coincident RTP magnetic anomaly with overlaid survey profiles.* ***(c, d)*** *MINEPLAT ultra-high-resolution seismic images across the Milfontes bathymetric high showing that it consists of an uplifted Paleozoic high controlled by a SW-NE striking fault, the Milfontes fault. The depth of D2 (top of Mesozoic sequence) is constrained by deep multichannel seismic data (GSI). The high amplitude and the shape of the Milfontes magnetic anomaly support the existence of a magmatic intrusion along the Milfontes fault, however, at depths not imaged by these seismic profiles.*

6.3. Melides magnetic lineament

A series of individual N-S aligned magnetic anomalies is observed north of Sines, defining the Melides magnetic lineament. The anomalies have amplitudes ranging from 100 to 500 nT and wavelengths about 0.8 - 1 km and lie along a ~4 km wide, 25 km long stretch parallel to the N-S direction. This lineament terminates against the offshore extension of the Grândola fault (**Figure 5, Figure 10, L6**, **Figure 13**, Figure 14).

Deep seismic data (GSI lines; **Figure 13**b,d) show that this magnetic lineament coincides with a fault zone that affects the whole Mesozoic sequence (F3 and F4 in **Figure 13**). The ultra-high-resolution seismic profiles (MP lines; **Figure 13**c; *Supplementary Figure S2*) show that the Cenozoic sequence hosts a series of vertical faults in the zone coincident with the positive magnetic anomaly (**Figure 13**c). Moreover, these profiles show a lateral variation of the seismic facies beneath the Lower Miocene unconformity D1 (i.e., in the Mesozoic units). To the west of the fault zone, D1 truncates steeply dipping reflectors of the regional Jurassic limestones strata (unit U1; **Figure 11**), while to the east and under the U3 faulted zone, the acoustic facies is transparent, consistent with a homogenous magmatic intrusion (unit U2). This is in agreement with reactivation of the rift fault, possibly enhanced by rheological heterogeneities associated with the intruded bodies.

The Melides N-S lineament is parallel to the main rift boundary fault of the Santiago do Cacém basin that also contains basic dikes (Inverno et al., 1993) and to the Setúbal-Pinhal Novo rift fault of Jurassic age, both of which have likely been active in Neogene and Quaternary times as left-lateral strike-slip faults (**Figure 1**; Figure 14) (Cabral et al., 2003).

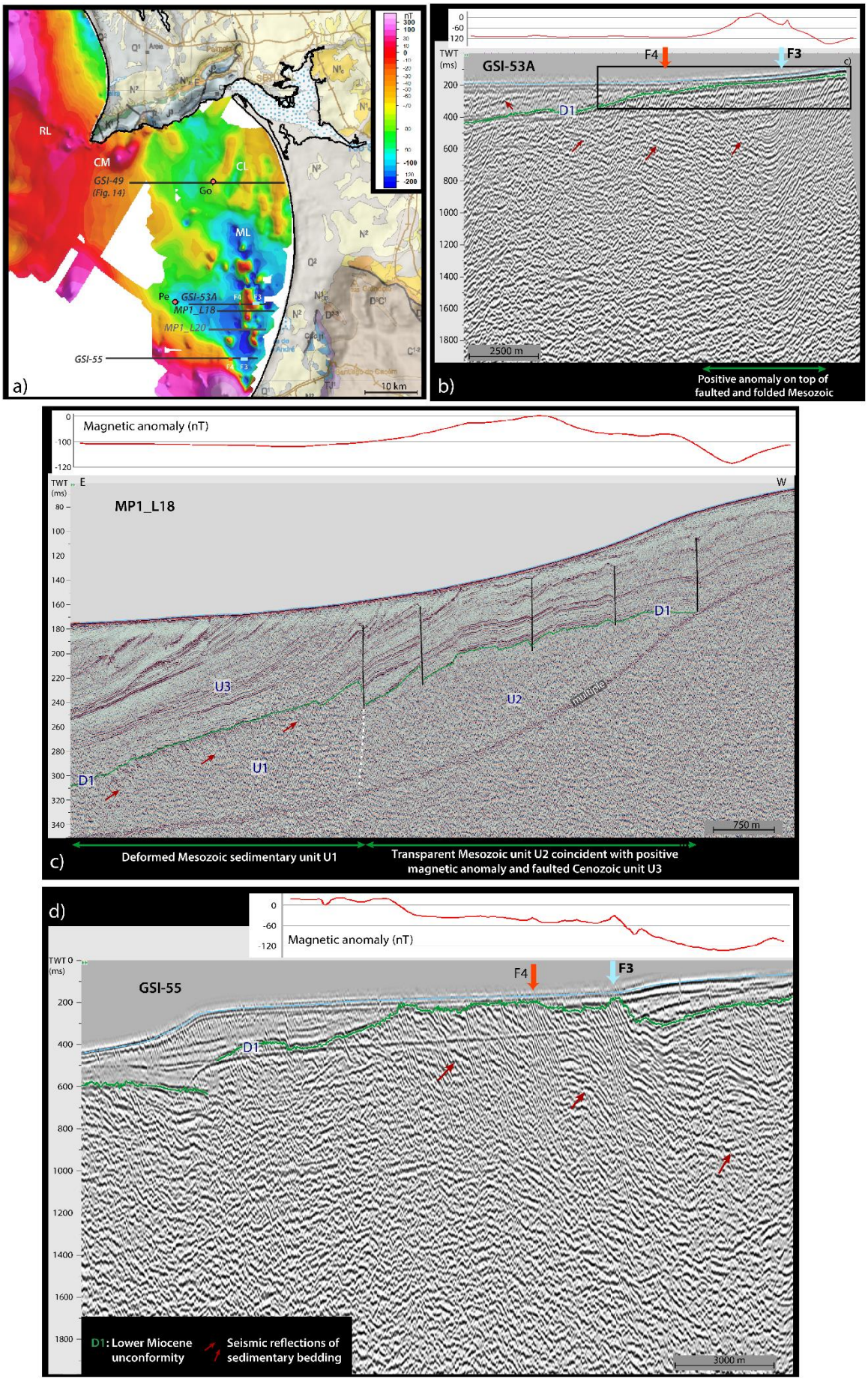

Figure 13*: Melides magnetic lineament and fault zone.* ***(a)*** *RTP magnetic anomaly map (located in* ***Figure 2****) with location of seismic profiles shown in this figure and in Figure 14. The color scale is enhanced for the showed region.*

(b, c, d) *Interpreted seismic profiles, with respective co-located magnetic anomaly profiles. The red arrows show the Mesozoic bedding reflectors. D1 is the Lower Miocene unconformity that truncates the Mesozoic sequence. F3 and F4 pinpoint faults deforming the Mesozoic units. These faults are identified in the seismic sections (b, d) and on the map on top of the respective lines in (a).*

(b) *Deep seismic line across the Melides lineament. Note the positive anomaly on top of F3. The black rectangle locates the equivalent location of the section shown in (c).*

(c) *Ultra-high-resolution profile across the Melides lineament. The lateral variation of the seismic facies distinguishes beneath D1: U1, deformed Mesozoic strata with steep bedding (Jurassic limestones;* ***Figure 11****); and U2, a transparent unit compatible with a homogenous magmatic intrusion. A series of vertical faults affect the Cenozoic strata of seismic unit U3 above U2, coincident with positive magnetic anomaly. The intrusion of U2 has deformed U1 and concentrated brittle deformation during the Cenozoic along the fault.*

(d) *Deep seismic line showing the seismic reflection image of the faults F3 and F4.*

ML: Melides lineament; CL: Comporta lineations (see Figure 14); RL: Roca-Espichel lineament; CM: Cova da Mijona anomaly; Go, Pe: Golfinho and Pescada wells. MP1_L20 seismic profile is shown as Supplementary Figure S2. See Figure 14 for structural interpretation.

6.4. Comporta anomaly zone and offshore Grândola fault

South of the Arrábida thrust belt, the anomaly field shows a smooth variation when compared with the other discussed zones (**Figure 13**), with the exception of the >110 nT Cova da Mijona anomaly (CM) (cf. Section 6.1, Figure 8a).

Nonetheless, a series of ~N-S trending anomalies, with low amplitude (~20 nT), ~2 km wavelength and 15-20 km length are identified (**Figure 13**), forming the Comporta anomaly zone. Despite their low amplitude, these lineations are clearly defined, standing out in the vertical and tilt derivatives (**Figure 7**). At south, this anomaly zone terminates against the offshore extension of the Grândola fault (Figure 14). Inspection of bathymetry and high-resolution MINEPLAT seismic data show that these anomalies have no relation with the Setúbal canyon or other recent sedimentary features. Instead, as shown in Figure 14, these anomalies seem to be associated with upright folds of the Mesozoic rocks induced by strike-slip deformation of Neogene age. In addition, to the west of the anomaly zone towards the Sesimbra canyon, the lower observed magnetic anomaly coincides with thicker Cenozoic sediments and deeper and less deformed Mesozoic (Figure 14b).

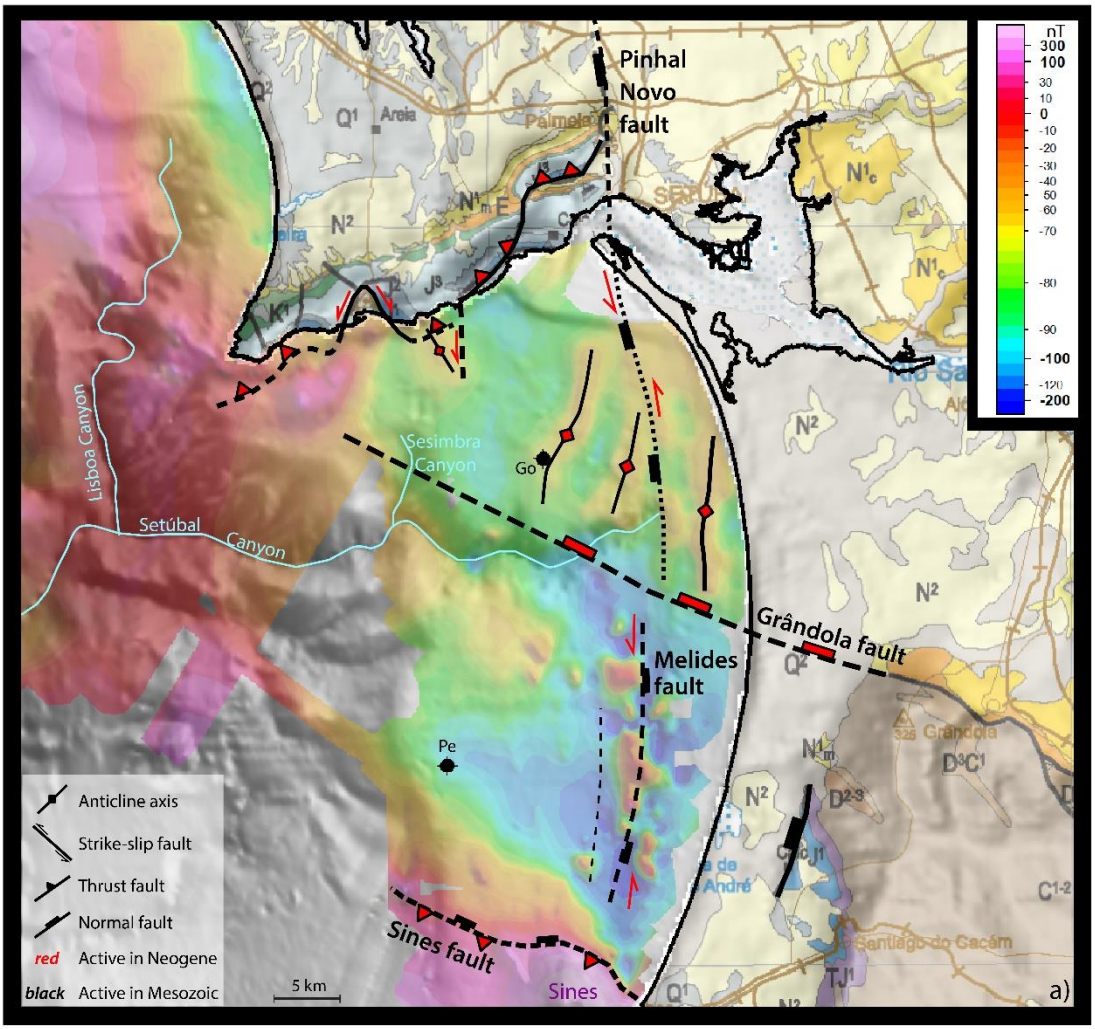

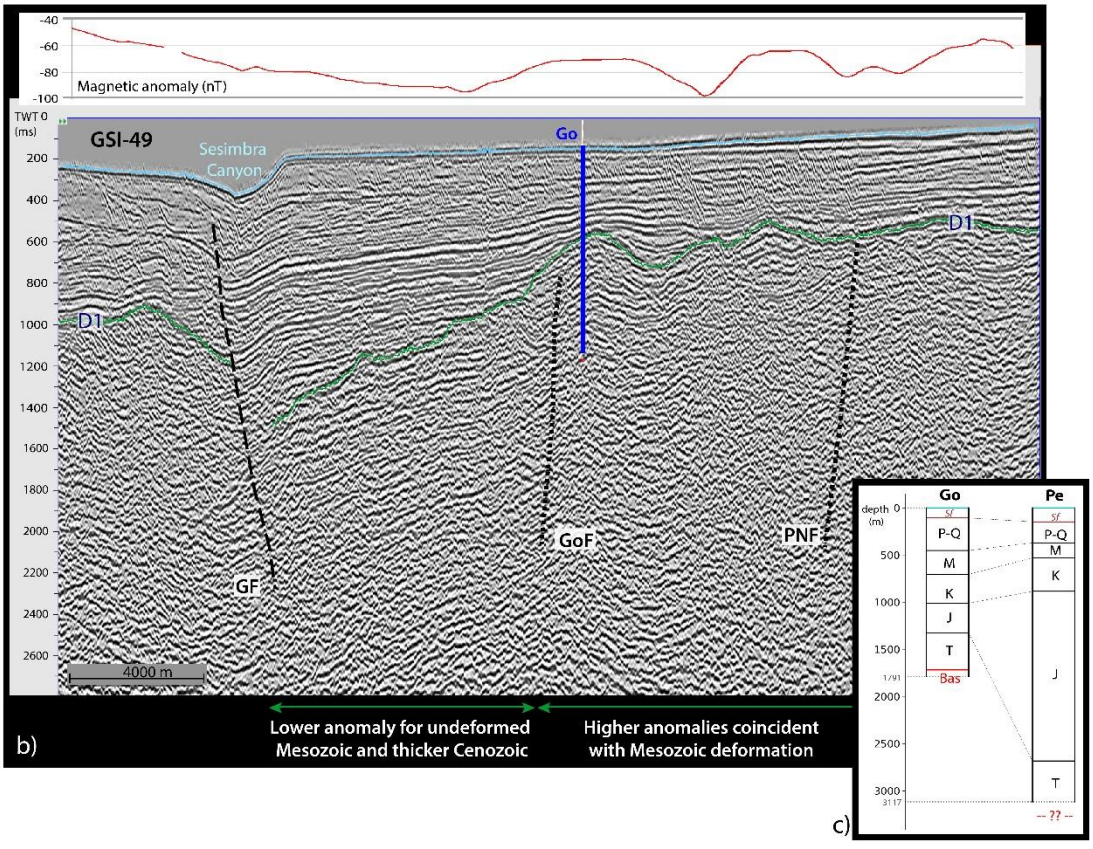

*Figure 14: Structural interpretation of the region north of Sines (**Figure 2** for location), based on the new magnetic map and other available data. **(a)** RTP magnetic anomaly is shown with transparency, overlaying the bathymetry. A series of low-amplitude (~20 nT) linear anomalies is observed with consistent ~2 km wavelength, 20 km length and aligned ~N-S direction, the Comporta magnetic anomaly zone. The southern limit of these anomalies allows inferring the offshore extension of the Grândola fault (GF). The Melides fault is mapped based on the interpretation of faults F3 and F4 and similar, as shown in **Figure 13**.*

***(b)** Interpreted seismic profile GSI-49 (location in **Figure 13**) and respective magnetic anomaly profile. The Comporta lineations coincide with the deformation structure of the Mesozoic sequence, associated with strike-slip fault system possibly intruded by basic dikes. Note that no relation exists with the Setúbal canyon or other sedimentary features. **(c)** Simplified logs of Go (Golfinho) and Pe (Pescada) oil-industry wells with 1791 m and 3117 m total penetration depth, respectively. P-Q: Plio-Quaternary; M: Miocene; K: Cretaceous; J: Jurassic; T: Triassic; Bas: Paleozoic basement (not reached in Pe). GF: Grândola fault; GoF: Golfinho fault; PNF: Pinhal Novo fault. Note that the Melides lineament and fault are parallel to the onshore rift fault that also contains basic dikes (Inverno et al., 1993).*

7. Discussion

7.1. 3D inversion models for the Sines, Côvo and Milfontes anomalies

3D inversion of magnetic anomaly data was performed for the area comprising the three main anomalies of the Alentejo shelf Sines, Côvo and Milfontes) to help constraining the approximate geometry of their magnetic sources. For details on the methodology refer to *Supplementary Text S2; Supplementary Figure S3*. The output susceptibility voxi are provided as *Supplementary Files S3 and S4*.

Figure 15 shows the results of the inversion modeling. The Sines, Côvo and Milfontes magmatic intrusions clearly stand out as high susceptibility bodies.

The **Milfontes** main source is modeled at depths between 5 and 2 km, with smaller-scale peaks reaching shallower depths close to the seafloor.

The **Sines** modeled source aligns in the prolongation of the onshore magmatic outcrop along the NW-SE direction. It shows a sharp vertical limit at its southern border, suggesting that it is limited by a vertical fault coinciding with the boundary between the Mesozoic rift basin and the Paleozoic basement. Its main volume (S>0.02 SI) extends from seafloor to ~4 km in depth, and contains several higher susceptibility (S> 0.06 SI) plug-like bodies. This structure resembles the Sintra pluton emplacement model, in which a less magnetic granitic laccolith intrusion was preceded by a series of basic sills and plugs (Terrinha et al., 2017), as well as the structure modeled for the Monchique intrusion, with gabbroic plugs surrounded by less magnetic magmatic rocks (Camargo, 2022).

The modeled solution for the **Côvo** intrusion is only partially resolved because the MINEPLAT survey was restricted to the continental shelf and the western end of the anomaly was not reached. Nevertheless, the inversion model allows estimating an extent of 10 km along the N-S direction and of more than 15 km along the E-W direction. A main western body extends from 2 to ~8 km of depth, with vertical finger-like bodies reaching 600 m below sea level. A second body ("deep Côvo") is modeled from 10 km

below sea level to the base of the model. The deep Côvo body is offset to the east of the main shallower body and some connection between them is suggested by the model, although it cannot be confidently constrained. These dimensions indicate that the Côvo pluton is likely the largest individual magnetic source of the West Portuguese Margin. For simplicity, only the three main bodies (Sines, Côvo, Milfontes) are shown in Figure 15a-d, although some other few smaller scattered bodies are also modeled in some areas. It is worthwhile noting that the inversion model resolves a sharply defined sill-like body extending to the north of Côvo. This body is included in Figure 15e and is interpreted as the Côvo sill. A larger data coverage is required to confirm and better constrain this body and its relationship with other magmatic intrusions. Nevertheless, this result suggests that large sill-like bodies may be present in the area and may have been responsible for important magma transport, as suggested for other locations (e.g. Cartwright & Møller Hansen, 2006; Galland et al., 2018; Magee et al., 2016).

Analysis of the modeled susceptibility distribution of each of the three main bodies (considering the volume with S>0.02 SI) gives mean values of 0.056 SI, 0.107 SI and 0.110 SI, and standard deviations of 0.038 SI, 0.070 SI and 0.069 SI for the Milfontes, Sines and Côvo bodies, respectively. The Sines and Côvo bodies have identical susceptibility distribution, significantly distinct from Milfontes that has about half of their mean susceptibility. This is compatible with similar magmatic origin for Sines and Côvo and a different one for Milfontes.

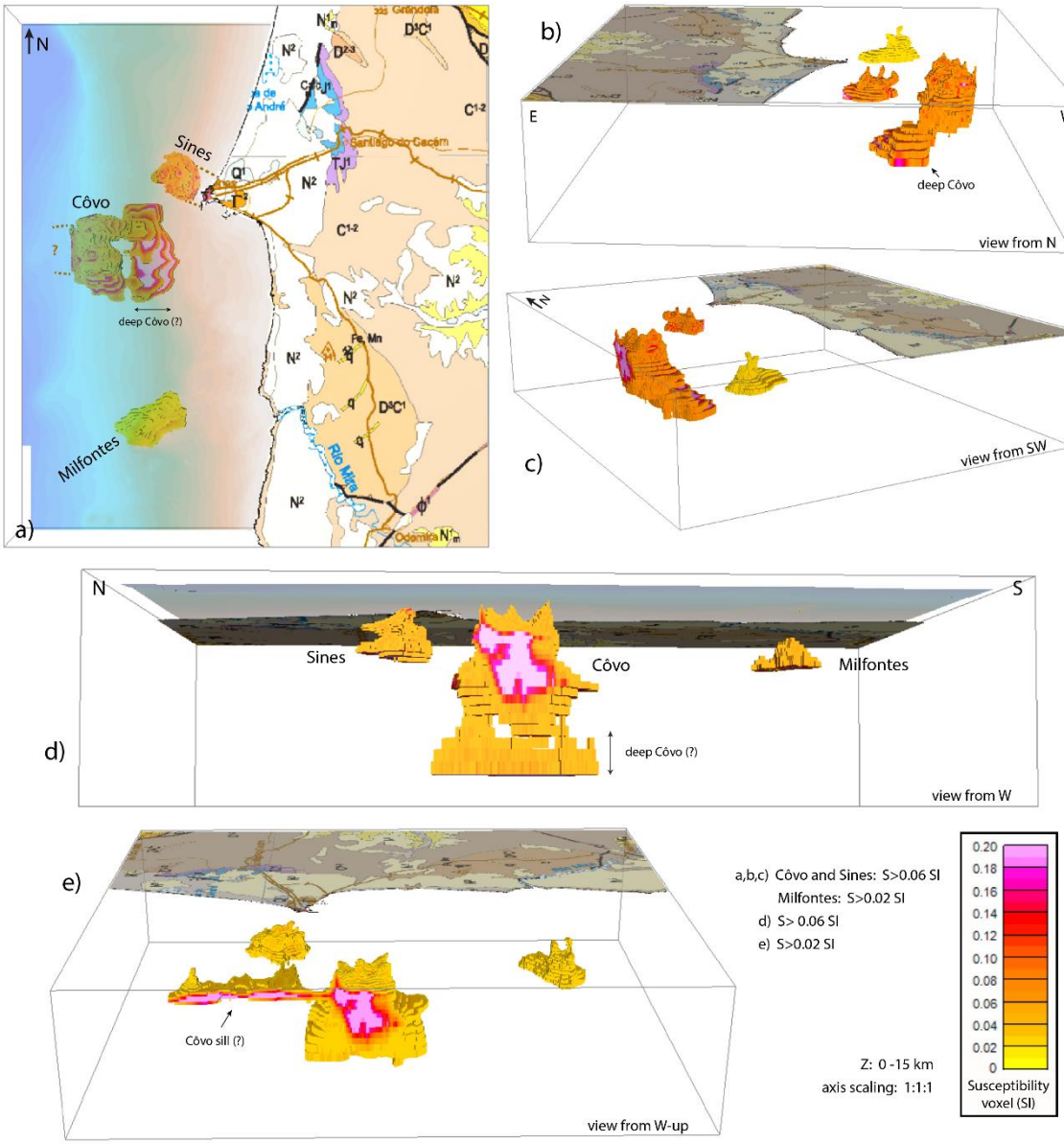

Figure 15: Results from the 3D susceptibility inversion models for the region of Sines, Côvo and Milfontes anomalies. The bottom depth of the model is 15 km deep. The shown bodies correspond to clipping of the output susceptibility model. Refer to the legend for the intervals of considered susceptibility. ***(a)*** *Map view of the three main bodies under transparent bathymetry grid.* ***(b-d)*** *Different perspective views showing the Sines, Côvo and Milfontes bodies. Note that Côvo is not totally modeled as it was only partially surveyed.* ***(e)*** *An additional horizontal sill-like modeled body is shown north of the Côvo intrusion (not shown in the other panels), suggesting the existence of a large-scale sill.*

7.2. High-resolution magnetic surveys as a tool to improve geological models

Figure 16a shows our survey data grid upward continued to 3000 m (**Figure 6c**) together with the 3000 m height aeromagnetic grid (Socias & Mezcua, 2002) (**Figure 1**d), to allow for direct comparison. The two datasets correlate well across the coastline, showing a large offshore extent of onshore magnetic anomalies. Notwithstanding we now know that the offshore anomaly field is more complex than imaged before**Figure 5**. This work shows that surveying the magnetic field at a much higher resolution and closer to the sources (e.g., high density marine surveys, in opposition to airborne) allows discriminating in much higher detail the shape and amplitude of individual anomalies, otherwise poorly resolved and underestimated (compare **Figure 16**a and **Figure 16**b). This was evident for the high amplitude and short wavelength anomalies of the Cabo Raso complex, and also for the larger wavelength Sines complex anomalies where distinguishing various bodies allowed attributing them to geological processes with very different ages and origins. High data quality is also essential to produce accurate 3D inversion models that allow estimating the geometry and volume of the sources. These models are important inputs for discussing the origin of the magmatic bodies that constitute the magnetic sources and the role of these in the geological evolution of the area.

The analysis of along-line data and derivative calculations (only accurate for good quality and resolution data) were decisive for identifying lower amplitude anomalies, allowing the correlation of anomalies measured in different lines and the definition of geologically meaningful lineations, such as for the Comporta lineations (Figure 14) and the Roca-Espichel fault (Figure 8, **Figure 7**).

On land, drone-borne close-to-surface magnetic surveys are a good solution to improve the detail magnetic anomaly mapping in areas of interest, such as done for the WILCAP Monchique intrusion (Camargo, 2022).

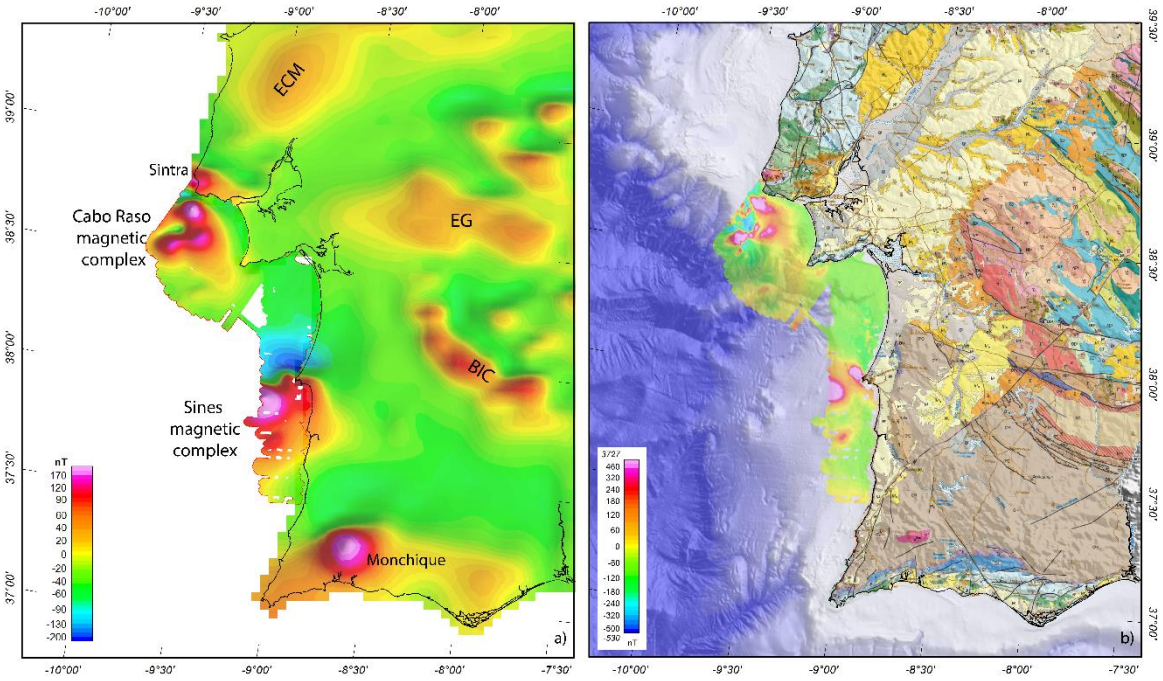

***Figure 16**: Regional integration of our new magnetic map. **(a)** Combination of the 3000 m upward continued survey data and the 3000 m height aeromagnetic grid (Socìas and Mezcua 2002), using the same color scale. The two datasets match across the coastline. Note that the upward continued field of the marine survey has similar wavelength anomalies as the aeromagnetic data, although with more detail in amplitude, due to the higher resolution of our marine survey. **(b)** Reduced to the pole anomaly (sea-level; **Figure 5**b) on top of bathymetry, and onshore geological map (1:10^6; https://geoportal.lneg.pt/).*

Main onshore magnetic anomalies: WILCAP Monchique magmatic intrusion; BIC: Beja igneous complex of metagabbro-dioritic rocks (Ossa Morena Zone); EG: Évora granitoid rocks (Ossa Morena Zone); ECM: Estremadura calcareous massif of Jurassic age. Note that no significant aeromagnetic anomaly is observed for the Iberian Pyrite Belt (that locates south of BIC).

7.3. Origin of the Magnetic Complexes of SW Iberia

The magnetic characteristics and the combined analysis with other geophysical methods allowed discussing the nature, age and tectonic relations of the different magnetic sources.

7.3.1. The Cabo Raso Magnetic Complex

The Cabo Raso anomaly is particularly interesting for historical reasons because it was already known by the Portuguese navigators in the XV century, due to the deflection that it caused in compasses when approaching at the Tagus River entrance.

The Cabo Raso magnetic complex comprises exhumed plutons (Figure 9) and deep-seated plutonic sources hosted in Mesozoic rift sediments, as well as a series of dikes and plugs of different shapes that extend to the southeast as far as the Arrábida thrust belt. These magmatic bodies are assigned to the WILCAP event, and a relation to the onshore plutonic and volcanic occurrences is evident.

The Guia anomaly has a NE-SW strike while the Cabo Raso one is parallel to NW-SE (Figure 8), which is also the strike of the main basic intrusion of the Sintra Magmatic Complex and the orientation of the connection with the Estremadura Spur. The Cova da Mijona intrusion is in line with a NE-SW striking onshore shale wall, hosted within a rift fault. The onshore complex of Cretaceous sills and dikes share the same orientations. Among these, stands out the NW-SE striking, ~30 km long dike that connects the E-Guia anomaly with the Cova da Mijona group of anomalies (Roca-Espichel fault zone). Both fault systems were inherited from the Paleozoic tectonics and re-worked during the Mesozoic rifting (Terrinha et al., 2019a).

7.3.2. The Sines magnetic Complex

To the south of Sines (~38ºN), magnetic anomalies correspond to magmatic bodies hosted in Paleozoic rocks (**Figure 10**a; **Figure 1**c). The high-resolution marine magnetic data presented here allow differentiating three main anomalies: Sines, Côvo and Milfontes that were previously assembled in one only (Carvalho et al., 1998) or barely distinguished (Miranda et al., 1989). From these, only the **Sines anomaly** has an onshore prolongation, the Late Cretaceous Sines Magmatic Complex (Miranda et al., 2009; Ribeiro et al., 2013) and thus can directly be assigned an Upper Cretaceous age.

In contrast, Côvo and Milfontes anomalies correspond to buried sources. The joint interpretation of the magnetic data, seismic profiles and multibeam bathymetry together with geological information support that neither the Côvo nor the Milfontes bodies are of Paleozoic age because of their setting and/or magnetic signature.

The Milfontes anomaly: a deep CAMP intrusion

Three hypotheses can be considered for the source of the Milfontes magnetic anomaly: firstly, metavolcanic rocks associated with the Paleozoic unit of the Iberian Pyrite Belt, present in the Cercal volcanic-siliceous complex (**Figure 1**b,c); secondly, intrusive rocks of the CAMP Triassic event; thirdly, intrusive rocks associated to the WILCAP. A Paleozoic origin is not likely because (i) it extends much wider than typical Paleozoic outcrops; (ii) its amplitude is about 10 times higher than the magnetic anomalies measured over equivalent mineralized metavolcanic rocks of the Iberian Pyrite Zone (Matos et al., 2020); (iii) its NE-SW elongation is not compatible with onshore Paleozoic anomalies that trend parallel to the NW-SE orogenic fabric (**Figure 1**c). A WILCAP origin is also discarded because (i) it does not fit the general NW-SE to W-E strike of the Late Cretaceous plutons on the West Portuguese Margin; (ii) its amplitude is ~5 times lower than the Late Cretaceous anomalies (**Figure 10**); (iii) its modeled bulk susceptibility (Section 7.1) is also significantly lower when compared to the susceptibility of known WILCAP sources (Section 7.1).

The NE-SW strike of the Milfontes anomaly and fault, prolongating along NE as a splay of dikes, is parallel to the 600 km long Messejana fault that outcrops 30 km SE of the Milfontes anomaly (**Figure 1**; **Figure 10**a) and both Milfontes and Messejana faults downthrow their NW-flank. The Messejana fault hosts a tholeiitic basaltic dike of Triassic age that is part of the CAMP event (Martins et al., 2008; Marzoli et al., 1999) and assigns to this fault a positive magnetic anomaly onshore (Matos et al., 2020; de Vicente et al., 2021). Hence, we favor a deep buried CAMP-related intrusion as the source for this anomaly. So far, the CAMP was only represented in West Iberia by the continuous onshore exposure of lava flows in south Portugal and by the 600 km long Messejana dike. Thus the Milfontes intrusion indicates the probable existence of plutonic

magma sources for the CAMP in Iberia, similarly to the plutonic sources in the lower crust that have been reported underlying the CAMP dike complex in the South Georgia Rift Basin using seismic refraction experiments (Marzen et al., 2020).

The Côvo intrusion

A Paleozoic origin for the Côvo intrusion is discarded, based on the much higher values of its magnetic anomaly (more than 10 times higher) when compared with the anomalies caused by very large bodies that outcrop onshore in the Paleozoic (e.g., Beja igneous complex; **Figure 16**).

A WILCAP source is favored based on its anomaly amplitude, which is compatible with other Late Cretaceous sources. The minor eccentricity of its shape is similar to the Monchique anomaly, also of Cretaceous age (**Figure 1**) (Camargo, 2022).

The 3D inversion susceptibility model (Section 7.1) shows > 10 km lateral extent, and points toward a deep extension of the intrusive body, suggesting two separate and offset bodies. These dimensions suggest that the Côvo plutonic intrusion is possibly the largest Mesozoic magmatic intrusion in West Iberia, being comparable in size with the Guadalquivir intrusion along the ocean-continent transition off southwest Iberia (Neres et al., 2018).

It is noteworthy that this is the first time that intrusions lying on the non-rifted margin are modeled at such depths, which is meaningful because the most active seismic swarm in SW Iberia lies below the Monchique intrusion between 5 and 20 km of depth (Camargo, 2022; Custódio et al., 2015). As a matter of fact some hypocenters nucleate in the region of Côvo (Custódio et al., 2015).

7.3.3. The Melides-Grândola anomalies

The linear, N-S trending anomalies near the coast between Sines (~38ºN) and the Arrábida thrust belt (~38º 30') are clearly associated to dikes and plugs intruding Jurassic-Cretaceous rift faults, as revealed by seismic multi-channel lines (**Figure 13**; Figure 14). Tectonic inversion of the rift basin in Cenozoic times re-worked these faults

as left-lateral transpressive faults, possibly enhanced by rheological heterogeneities associated with the intruded bodies. The anticlinal folds form positive magnetic anomalies likely indicating the existence of basic dikes and plugs as in other parts of the Lusitanian Basin (Mata et al., 2015; Miranda et al., 2009; Terrinha et al., 2017). These intrusive bodies are assigned to the WILCAP event. A CAMP origin is excluded because they intrude Cretaceous-Jurassic sediments, and a relation to the second pulse of magmatism (~145 Ma) is also not likely due to its restricted geographic location to the northern Lusitanian basin.

7.4. Tectonic control of magmatic events

Except for the Côvo pluton (which has not been fully mapped), all the mapped intrusions were emplaced within recognized faults: NW-SE striking Variscan and NE-SW Late Variscan faults, which have been re-activated during the Mesozoic rifting, and also N-S striking Mesozoic rifting faults. Because the Cabo Raso plutons as well as the dike systems of the WILCAP used both NE-SW and NW-SE striking faults, it is likely that most of these intrusions used the pre-existent tectonic grain during a period of quiescent tectonics.

Although the geochemistry of the CAMP and WILCAP bodies indicate the lithospheric mantle as magmatic source (Miranda et al., 2009), it appears that the location and geometry of the intrusions are controlled by the crustal tectonic fabric, possibly detaching at a deep level, such as the Moho. Moreover, the identified magnetic anomalies correspond, in the studied cases, to magmatic bodies that have later nucleated strain associated with the post-rifting Alpine tectonic inversion of the rift basins.

8. Conclusions

The West Iberia margin evolved from a magma-poor rifted margin. Notwithstanding, the margin hosted two main magmatic events, the Late Triassic Central Atlantic Magmatic Province (CAMP) and the Late Cretaceous Alkaline Province (WILCAP). Based on original geophysical surveys with high-resolution magnetic and acoustic data on the continental shelf and slope, this work brings important insights for the understanding of these events and their relation with the West Iberia tectonic history.

The higher resolution of our marine surveys, when compared with the low-resolution and high-altitude aerial surveys, allowed mapping anomalies with much higher accuracy and to define magnetic complexes. These complexes correspond to zones previously seen as single blurred anomalies that we now show to comprise various magnetic sources, in some cases due to non-coeval magmatic events.

The detailed mapping of the Cabo Raso anomaly zone reveals that this region hosts a complex plutonic and sub-volcanic system with large volumes of intruded magma. The Côvo and Milfontes plutons as well as the Melides-Grândola linear anomalies and the Cabo Espichel anomalies (dikes and plugs) are new findings. The Côvo intrusion is possibly the largest Mesozoic pluton in west Portugal. The Milfontes anomaly is the first evidence of a significant plutonic source of the CAMP in Iberia. The crustal fabric inherited from the Paleozoic Variscan orogeny, re-worked during the Mesozoic rifting and the Cenozoic Alpine orogeny, was the main tectonic control for the magmatic intrusions. The magmatic bodies may have affected the rheological structure of the crust, and thus the strain localization during the Alpine collision and recent tectonics.

Data availability

Magnetic data used in this work were acquired and processed by our team, as described in sections 4 and 5 of the manuscript. Magnetic anomaly grids (full processed) are available at https://doi.org/10.5281/zenodo.7825216.

Bathymetry data was downloaded from www.emodnet-bathymetry.eu and topography from https://www.ngdc.noaa.gov/mgg/global/. Geological maps were downloaded from https://geoportal.lneg.pt/en/opendata/geological_maps/. Metadata of the MINEPLAT seismic surveys can be found at https://divgmwebgis.ipma.pt/ and data can be accessed on request.

Acknowledgements

This work was funded by the Portuguese Fundação para a Ciência e a Tecnologia (FCT) I.P./MCTES through national funds (PIDDAC) – UIDB/50019/2020–IDL, UIDB/04292/2020–MARE, UIDB/04683/2020–ICT, MINEPLAT (ALT20-03-0145-FEDER-000013), PRORIFT (NSFC/0003/2016) and LISA (PTDC/CTA-GEF/1666/2020). MN acknowledges FCT for a post-doc grant SFRH/BPD/96829/2013 and junior researcher contract on the frame of TAGUSGAS project (PTDC/CTA-GEO/31885/2017).

Magnetic data processing and interpretation was done using a research license of *Oasis montaj* (Geosoft). The industry GSI seismic data was made available by DGEG (Direcção Geral de Energia e Geologia) to whom we acknowledge, particularly José Miguel Martins. All data are reproduced with full legal permission. This work was possible due to the IPMA's SEISLAB infrastructure funded by C4G (Collaboratorium for Geosciences).

We are indebted to EMEPC (Portuguese Task Force for the Extension of the Continental Platform) for magnetometer lending whenever requested and for making possible and conducting the ROCHEL and CHELSI surveys aboard the RV Selvagem Grande. Special

thanks to the pilots António Calado, Andreia Afonso and Bruno Ramos. We also thank the crews of IPMA's Noruega and Diplodus research vessels.

We thank Guilherme Madureira for the maintenance of IPMA's São Teotónio magnetic base station. We thank the Observatório Geofísico e Astronómico da Universidade de Coimbra, OGAUC (https://www.uc.pt/org/observatorio/observacoes), especially Paulo Ribeiro, for providing magnetic data from the COI observatory. We acknowledge the Instituto Geografico Nacional, Spain, for supporting the operation of the San Pablo – Toledo INTERMAGNET geomagnetic observatory (www.intermagnet.org). We thank José Manuel Tordesillas from the Observatório Geofísico de Toledo for making available the compilation of Iberia aeromagnetic data.

We thank Nick Schofield and another anonymous reviewer, the Associate Editor Augusto Rapalini, and the Editor Taylor Schildgen, for positive and constructive comments on our manuscript.

References

Allan, T. D. (1965). A magnetic survey off the Coast of Portugal. *Geophysics*, *30*(3). https://doi.org/10.1190/1.1439594

Alves, T. M., Gawthorpe, R. L., Hunt, D. W., & Monteiro, J. H. (2003). Cenozoic tectono-sedimentary evolution of the western Iberian margin. *Marine Geology*, *195*(1–4). https://doi.org/10.1016/S0025-3227(02)00683-7

Alves, T. M., Moita, C., Cunha, T., Ullnaess, M., Myklebust, R., Monteiro, J. H., & Manuppella, G. (2009). Diachronous evolution of late jurassic-cretaceous continental rifting in the northeast atlantic (west iberian margin). *Tectonics*, *28*(4). https://doi.org/10.1029/2008TC002337

Ardizone, J., Mezcua, J., & Socias, I. (1989). Mapa Aeromagnetico de España Peninsular. Instituto Geográfico Nacional, Spain.

Arthaud, F., & Matte, P. (1977). Late Paleozoic strike-slip faulting in southern Europe and northern Africa: Result of a right-lateral shear zone between the Appalachians and the Urals. *Geological Society of America Bulletin*, *88*(9), 1305–1320.

Barbosa, S. (1999). *Estudo geoestatítico de dados experimentais da anisotropia da susceptibilidade magnética de rochas do maciço de Monchique*. MSc thesis, Universidade do Porto, Portugal.

Blakely, R. J. (1996). *Potential Theory in Gravity and Magnetic Applications*. *Potential Theory in Gravity and Magnetic Applications*. Cambridge University Press. https://doi.org/10.1017/cbo9780511549816

Cabral, J., Moniz, C., Ribeiro, P., Terrinha, P., & Matias, L. (2003). Analysis of seismic reflection data as a tool for the seismotectonic assessment of a low activity intraplate basin–the Lower Tagus Valley (Portugal). *Journal of Seismology*, *7*(4), 431–447.

Camargo, G. (2022). *Magnetic and gravimetric modeling of the Monchique magmatic intrusion in south Portugal*. MSc thesis, Universidade de Lisboa, Portugal. http://hdl.handle.net/10451/54221.

Campbell, D. L. (1978). Investigation of the stress-concentration mechanism for intraplate earthquakes. *Geophysical Research Letters*, *5*(6), 477–479.

Cartwright, J., & Møller Hansen, D. (2006). Magma transport through the crust via interconnected sill complexes. *Geology*, *34*(11), 929–932.

Carvalho, J. P. G., Torres, L. M., & Afilhado, A. (1998). Delimitação do maciço sub-vulcânico de Sines offshore a partir de dados geofísicos. *Comum. Serv. Geol. Port*, *84*, D57–D60.

Civiero, C., Custódio, S., Neres, M., Schlaphorst, D., Mata, J., & Silveira, G. (2021). The Role of the Seismically Slow Central-East Atlantic Anomaly in the Genesis of the Canary and Madeira Volcanic Provinces. *Geophysical Research Letters*, *48*(13), e2021GL092874.

Custódio, S., Dias, N. A., Carrilho, F., Góngora, E., Rio, I., Marreiros, C., et al. (2015). Earthquakes in western Iberia: improving the understanding of lithospheric deformation in a slowly deforming region. *Geophysical Journal International*, *203*(1), 127–145.

Dias, R., Oliveira, J. T., Matos, J. ., Ressurreição, R., Pereira, Z., Machado, S., et al. (2016). Notícia explicativa da folha 42-A Grândola. Laboratório Nacional de Energia e Geologia, Portugal. Retrieved from www.lneg.pt

Ellis, R. G., de Wet, B., & Macleod, I. N. (2012). Inversion of magnetic data for remanent and induced sources. In *ASEG Extended Abstracts, pp. 1-4*.

Escada, C., Represas, P., Santos, F., Pereira, R., Mata, J., & Rosas, F. M. (2022). New evidence of Late Cretaceous magmatism on the offshore central West Iberian Margin (Estremadura Spur) from potential field data. *Tectonophysics*, *832*, 229354. https://doi.org/10.1016/J.TECTO.2022.229354

Font, E., Fernandes, S., Neres, M., Carvallo, C., Martins, L., Madeira, J., & Youbi, N. (2015). Paleomagnetism of the Central Atlantic Magmatic Province in the Algarve basin, Portugal: First insights. *Tectonophysics*, *663*. https://doi.org/10.1016/j.tecto.2015.07.036

Fraga, T., Fonseca, C., Coelho, I. P., Freire, J., Carvalho, P. C. S. de, & Teixeira, A. (2015). Research in maritime archaeology in Portugal. In *Shipwrecks around the World* (pp. 450–485). Prestige Books.

Galland, O., Bertelsen, H. S., Eide, C. H., Guldstrand, F., Haug, Ø. T., Leanza, H. A., et al. (2018). Chapter 5 - Storage and Transport of Magma in the Layered Crust—Formation of Sills and Related Flat-Lying Intrusions. In S. B. T.-V. and I. P. S.

Burchardt (Ed.) (pp. 113–138). Elsevier. https://doi.org/https://doi.org/10.1016/B978-0-12-809749-6.00005-4

Geldmacher, J., Hoernle, K., Klügel, A., v.d. Bogaard, P., Wombacher, F., & Berning, B. (2006). Origin and geochemical evolution of the Madeira-Tore Rise (eastern North Atlantic). *Journal of Geophysical Research: Solid Earth*, *111*(9). https://doi.org/10.1029/2005JB003931

Grange, M., Scharer, U., Merle, R., Girardeau, J., & Cornen, G. (2010). Plume-lithosphere interaction during migration of cretaceous alkaline magmatism in SW Portugal: Evidence from U-Pb Ages and Pb-Sr-Hf isotopes. *Journal of Petrology*, *51*(5). https://doi.org/10.1093/petrology/egq018

Inverno, C., Manuppella, G., Zbyszewski, G., & Pais, J. (1993). Notícia explicativa da folha 42-C Santiago do Cacém. Serviços Geológicos de Portugal. Retrieved from www.lneg.pt

Kullberg, M. C., Kullberg, J. C., & Terrinha, P. (2000). Tectónica da cadeia da Arrábida. *Mem. Mus. Nac. Hist. Nat., Nº 2*. Retrieved from http://hdl.handle.net/10362/5413

Magee, C., Muirhead, J. D., Karvelas, A., Holford, S. P., Jackson, C. A. L., Bastow, I. D., et al. (2016). Lateral magma flow in mafic sill complexes. *Geosphere*, *12*(3), 809–841.

Martins, L. T., Madeira, J., Youbi, N., Munhá, J., Mata, J., & Kerrich, R. (2008). Rift-related magmatism of the Central Atlantic magmatic province in Algarve, Southern Portugal. *Lithos*, *101*(1–2). https://doi.org/10.1016/j.lithos.2007.07.010

Marzen, R. E., Shillington, D. J., Lizarralde, D., Knapp, J. H., Heffner, D. M., Davis, J. K., & Harder, S. H. (2020). Limited and localized magmatism in the Central Atlantic Magmatic Province. *Nature Communications*, *11*(1), 3397. https://doi.org/10.1038/s41467-020-17193-6

Marzoli, A., Renne, P. R., Piccirillo, E. M., Ernesto, M., Bellieni, G., & De Min, A. (1999). Extensive 200-million-year-old continental flood basalts of the Central Atlantic Magmatic Province. *Science*, *284*(5414). https://doi.org/10.1126/science.284.5414.616

Mata, J., Alves, C. F., Martins, L., Miranda, R., Madeira, J., Pimentel, N., et al. (2015). 40Ar/39Ar ages and petrogenesis of the West Iberian Margin onshore magmatism at the Jurassic-Cretaceous transition: Geodynamic implications and assessment of open-system processes involving saline materials. *Lithos*, *236–237*. https://doi.org/10.1016/j.lithos.2015.09.001

Matos, J., Carvalho, J., Represas, P., Batista, M., Sousa, P., Ramalho, E., et al. (2020). Geophysical surveys in the Portuguese sector of the Iberian Pyrite Belt: a global overview focused on the massive sulphide exploration and geologic interpretation. *Comunicações Geológicas*, *107*, 41–78.

Merle, R., Schärer, U., Girardeau, J., & Cornen, G. (2006). Cretaceous seamounts along the continent-ocean transition of the Iberian margin: U-Pb ages and Pb-Sr-Hf isotopes. *Geochimica et Cosmochimica Acta*, *70*(19). https://doi.org/10.1016/j.gca.2006.07.004

Merle, R., Jourdan, F., & Girardeau, J. (2018). Geochronology of the Tore-Madeira Rise

seamounts and surrounding areas: a review. *Australian Journal of Earth Sciences*. https://doi.org/10.1080/08120099.2018.1471005

Mil-Homens, M., Brito, P., Magalhães, V., Rosa, M., Neres, M., Silva, M., et al. (2020). Integrated geophysical and sedimentological datasets for assessment of offshore borrow areas: the CHIMERA project (western Portuguese Coast). *Geological Society, London, Special Publications*, *505*, SP505-2019–100. https://doi.org/10.1144/SP505-2019-100

Miranda, J. M., Galdeano, A., Rossignol, J. C., & Mendes Victor, L. A. (1989). Aeromagnetic anomalies in mainland Portugal and their tectonic implications. *Earth and Planetary Science Letters*, *95*(1–2). https://doi.org/10.1016/0012-821X(89)90174-X

Miranda, R., Valadares, V., Terrinha, P., Mata, J., Azevedo, M. do R., Gaspar, M., et al. (2009). Age constraints on the Late Cretaceous alkaline magmatism on the West Iberian Margin. *Cretaceous Research*, *30*(3). https://doi.org/10.1016/j.cretres.2008.11.002

Nabighian, M. N. (1972). The analytic signal of two-dimensional magnetic bodies with polygonal cross-section: its properties and use for automated anomaly interpretation. *Geophysics*, *37*(3), 507–517.

Nance, R. D., Gutiérrez-Alonso, G., Keppie, J. D., Linnemann, U., Murphy, J. B., Quesada, C., et al. (2012). A brief history of the Rheic Ocean. *Geoscience Frontiers*, *3*(2), 125–135. https://doi.org/https://doi.org/10.1016/j.gsf.2011.11.008

Neres, M., Font, E., Miranda, J. M., Camps, P., Terrinha, P., & Mirão, J. (2012). Reconciling Cretaceous paleomagnetic and marine magnetic data for Iberia: New Iberian paleomagnetic poles. *Journal of Geophysical Research: Solid Earth*, *117*(6). https://doi.org/10.1029/2011JB009067

Neres, M., Bouchez, J. L., Terrinha, P., Font, E., Moreira, M., Miranda, R., et al. (2014). Magnetic fabric in a Cretaceous sill (Foz da Fonte, Portugal): Flow model and implications for regional magmatism. *Geophysical Journal International*, *199*(1). https://doi.org/10.1093/gji/ggu250

Neres, M., Terrinha, P., Custódio, S., Silva, S. M., Luis, J., & Miranda, J. M. (2018). Geophysical evidence for a magmatic intrusion in the ocean-continent transition of the SW Iberia margin. *Tectonophysics*, *744*. https://doi.org/10.1016/j.tecto.2018.06.014

Noiva, J., Ribeiro, C., Terrinha, P., Neres, M., & Brito, P. (2017). Exploring the alentejo continental shelf for minerals and plio-quaternary environmental changes: Preliminary results of the mineplat survey. *Comunicacoes Geologicas*, *104*(1). Retrieved from http://hdl.handle.net/10174/25610

Oehler, J. F., & Lequentrec-Lalancette, M. F. (2019). The contribution of marine magnetics in the Gulf of Saint-Malo (Brittany, France) to the understanding of the geology of the North Armorican Cadomian belt. *Comptes Rendus - Geoscience*, *351*(1). https://doi.org/10.1016/j.crte.2018.10.002

Oliveira, J. T., Quesada, C., Pereira, Z., Matos, J. X., Solá, A. R., Rosa, D., et al. (2019). South Portuguese Terrane: A Continental Affinity Exotic Unit BT - The Geology of Iberia: A Geodynamic Approach: Volume 2: The Variscan Cycle. In C. Quesada &

J. T. Oliveira (Eds.) (pp. 173–206). Cham: Springer International Publishing. https://doi.org/10.1007/978-3-030-10519-8_6

Pais, J., Cunha, P. P., Pereira, D., Legoinha, P., Dias, R., Moura, D., et al. (2012). The Paleogene and Neogene of Western Iberia (Portugal): A Cenozoic Record in the European Atlantic Domain. https://doi.org/10.1007/978-3-642-22401-0_1

Palencia Ortas, A., Osete, M. L., Vegas, R., & Silva, P. (2006). Paleomagnetic study of the Messejana Plasencia dyke (Portugal and Spain): A lower Jurassic paleopole for the Iberian plate. *Tectonophysics*, *420*(3), 455–472. https://doi.org/https://doi.org/10.1016/j.tecto.2006.04.003

Pereira, R., Rosas, F., Mata, J., Represas, P., Escada, C., & Silva, B. (2021). Interplay of tectonics and magmatism during post-rift inversion on the central West Iberian Margin (Estremadura Spur). *Basin Research*, *33*(2), 1497–1519.

Portniaguine, O., & Zhdanov, M. S. (2002). 3-D magnetic inversion with data compression and image focusing. *Geophysics*, *67*(5), 1532–1541. https://doi.org/10.1190/1.1512749

Quesada, Braid, J. A., Fernandes, P., Ferreira, P., Jorge, R. S., Matos, J. X., et al. (2019). SW Iberia Variscan Suture Zone: Oceanic Affinity Units. https://doi.org/10.1007/978-3-030-10519-8_5

Ribeiro, A. (2002). *Soft Plate and Impact Tectonics*. *Soft Plate and Impact Tectonics*. https://doi.org/10.1007/978-3-642-56396-6

Ribeiro, P., Silva, P. F., Moita, P., Kratinová, Z., Marques, F. O., & Henry, B. (2013). Palaeomagnetism in the Sines massif (SW Iberia) revisited: Evidences for late cretaceous hydrothermal alteration and associated partial remagnetization. *Geophysical Journal International*, *195*(1). https://doi.org/10.1093/gji/ggt261

Rock, N. M. S. (1982). The Late Cretaceous Alkaline Igneous Province in the Iberian Peninsula, and its tectonic significance. *LITHOS*, *15*(2). https://doi.org/10.1016/0024-4937(82)90004-4

Silva, P. F., Henry, B., Marques, F. O., Font, E., Mateus, A., Vegas, R., et al. (2008). Magma flow, exsolution processes and rock metasomatism in the Great Messejana–Plasencia dyke (Iberian Peninsula). *Geophysical Journal International*, *175*(2), 806–824. https://doi.org/10.1111/j.1365-246X.2008.03920.x

Simões, P., Neres, M., & Terrinha, P. (2020). Joint modeling of seismic, magnetic and gravimetric data unravels the extent of the Late Cretaceous Magmatic Province on the Estremadura Spur offshore West Iberia. In *EGU General Assembly Conference Abstracts* (p. 571).

Soares, A. M. da C. (2018). *Caracterização da actividade sísmica de Monchique*. M.Sc. thesis, Faculdade de Ciências da Universidade de Lisboa. Retrieved from http://hdl.handle.net/10451/35535

Socias, I., & Mezcua, J. (2002). Mapa de Anomalias Magneticas de la Peninsula Ibérica. *Boletín Informativo Del Instituto Geográfico Nacional, Nº 9*. Instituto Geográfico Nacional, Spain.

Socias, I., & Mezcua, J. (2002). Mapa de Anomalias Magneticas de la Peninsula Ibérica. Boletín Informativo Del Instituto Geográfico Nacional, No 9. Instituto Geográfico

Nacional, Spain.

Tarling, D., & Hrouda, F. (1993). *Magnetic anisotropy of rocks*. Springer Science & Business Media.

Terrinha, P., Pueyo, E. L., Aranguren, A., Kullberg, J. C., Kullberg, M. C., Casas-Sainz, A., & Azevedo, M. do R. (2017). Gravimetric and magnetic fabric study of the Sintra Igneous complex: laccolith-plug emplacement in the Western Iberian passive margin. *International Journal of Earth Sciences*, *107*(5). https://doi.org/10.1007/s00531-017-1573-7

Terrinha, P., Ramos, A., Neres, M., Valadares, V., Duarte, J., Martínez-Loriente, S., et al. (2019a). The Alpine Orogeny in the West and Southwest Iberia Margins. https://doi.org/10.1007/978-3-030-11295-0_11

Terrinha, P., Duarte, H., Brito, P., Noiva, J., Ribeiro, C., Omira, R., et al. (2019b). The Tagus River delta landslide, off Lisbon, Portugal. Implications for Marine geo-hazards. *Marine Geology*, *416*. https://doi.org/10.1016/j.margeo.2019.105983

Thébault, E., Finlay, C. C., Beggan, C. D., Alken, P., Aubert, J., Barrois, O., et al. (2015). International Geomagnetic Reference Field: the 12th generation. *Earth, Planets and Space*, *67*(1), 79. https://doi.org/10.1186/s40623-015-0228-9

de Vicente, G., Olaiz, A., Muñoz-Martín, A., & Cunha, P. P. (2021). Longest and still longer: The Messejana-Plasencia dyke and its links with later Alpine deformation belt in Iberia. *Tectonophysics*, *815*, 229009.

Vinhas da Costa, A. (2018). *Estratigrafia sísmica da plataforma continental ao largo da cadeia da Arrábida-contributo para o conhecimento da evolução pós-miocénica*. MSc thesis, Faculdade de Ciências da Universidade de Lisboa, http://hdl.handle.net/10451/35675.

(Ellis et al., 2012; Portniaguine & Zhdanov, 2002)

AGU PUBLICATIONS

Tectonics

Supporting Information for

New Late Cretaceous and CAMP magmatic sources off West Iberia, from high-resolution magnetic surveys on the continental shelf

Marta Neres[1,2], Pedro Terrinha[1,2], João Noiva[1], Pedro Brito[1], Marcos Rosa[1], Luis Batista[1], Carlos Ribeiro[3,4,5]

1 IPMA - Instituto Português do Mar e da Atmosfera, 1749-077 Lisboa, Portugal
2 Instituto Dom Luiz, Faculdade de Ciências, Universidade de Lisboa, 1749-016 Lisboa, Portugal
3 Department of Geosciences, School of Science and Technology, University of Evora, Portugal
4 ICT - Institute of Earth Sciences, University of Évora, Portugal
5 MARE - Marine and Environmental Sciences Center, University of Évora, Portugal

Contents of this file

Additional Supporting Information

Text S1.

Seismic data

We use seismic data to better constrain the significance and interpretation of magnetic anomalies and anomaly zones (Figures 9, 13, 14, S2). The respective non-interpreted sections are presented in Supplementary Figures S4 to S12.

The studied and interpreted seismic profiles come from different datasets with distinct characteristics: from margin-scale, deep penetration and low resolution seismics acquired by the oil industry, to ultra-high resolution and low penetration academic surveys acquired only at shelf depths.

The reference of each seismic line is indicated in each respective figure, and includes the name of the survey (GSI, MP, TD or PM) and the reference number of the line within the survey. For instance, Figure 13c shows MP1-L18, i.e., line L18 of the MINEPLAT-1 survey.

We next describe the main technical specifications of the seismic acquisition and processing of the presented profiles.

- **GSI**

Deep penetration multichannel industry seismic profiles acquired and processed by the oil industry along the Portuguese margin, in 1984.

Acquisition parameters: streamer length: 3000 m; number of channels: 120; total air gun source volume: 2775 in^3; shot interval: 25 m; sample rate: 500 Hz (2 ms).

Main processing steps comprised: resampling to 4 ms, true amplitude recovery, pre-stack deconvolution, velocity analysis with 2 km spacing, stack, post-stack deconvolution, F-K migration and time-variant band-pass filter. The resulting seismic sections for interpretation have a central mean frequency of 15 to 30 Hz with CMP (common mid-point) spacing of 12.5m.

- **MINEPLAT (MP)**

Ultra-high resolution multichannel academic seismic profiles acquired and processed by IPMA (our team) during several surveys in 2016-2019, offshore the Alentejo region (Figure 1).

Acquisition parameters: streamer active section: 75 m; number of channels: 24; 200 tips sparker source with energy of 400 J; shot interval: 0.5 s; sample rate: 10000 Hz (0.1 ms).

Main processing steps comprised: pre-stack predictive deconvolution, static residuals picking and correction by common offset spatial averaging, interactive velocity analysis, stack, zero offset multiple attenuation, post-stack Kirchhoff time migration and time-variant band-pass filter. The resulting seismic sections for interpretation have a central mean frequency of 800 to 1200 Hz, average vertical resolution of 0.25 to 0.4 m, horizontal resolution (CMP spacing) of 1.6 m, and signal penetration up to 200 ms below the seabed.

- **TAGUSDELTA (TD)**

Ultra-high resolution multichannel academic seismic profiles acquired and processed by IPMA (our team) in 2011 in the Tagus delta area, offshore Cascais.

Acquisition and processing parameters similar to the MINEPLAT dataset.

- **PACEMAKER (PM)**

Single-channel academic seismic profiles acquired and processed by IPMA (our team) in 2011 in the Tagus delta area, offshore Cascais.

Acquisition parameters: 400 tips sparker source with energy of 0.5 to 1 kJ; shot interval: 1 s; sample rate: 10000 Hz (0.1 ms).

Main processing steps comprised: denoise, swell static corrections, Kirchhoff time migration and band-pass filtering. The signal frequency bandwidth ranged from 500 to 3500 Hz corresponding to decimeter vertical resolution, CMP spacing is 2 m, and signal penetration is up to 200 ms below the seabed.

Metadata of the seismic surveys can be found at https://divgmwebgis.ipma.pt/ and data can be further accessed upon request.

Text S2.

Magnetic inversion model

We ran 3D inversion models (Figure 15) to estimate the 3D susceptibility distribution of the magnetic sources for the Sines, Côvo and Milfontes anomalies. We used the VOXI program of Seequent (Ellis et al., 2012), following the methodology described by Neres et al. (2018).

To allow the maximum model resolution possible, we ran two independent models, for the Sines-Côvo anomalies region and for Milfontes area (red and blue polygons in Supplementary Figure S3, respectively). The models' geometry was defined by (x,y,z) meshes of 248 × 245 × 49 voxels with 100m, 150m and 50m side lengths for Sines-Côvo; and 243 × 246 × 46 voxels with 90m, 105m and 50m side lengths for Milfontes. The top of the model was constrained by the bathymetry and the bottom was restricted to 15 km.

We used as input data the sea-level magnetic anomaly grid (Figure 5a), and as inducing field the local IGRF: 43600 nT magnitude; 52° inclination; -2° declination. The initial model was S=0 for all voxels. The inverted susceptibility model was restricted to [0, 0.2] SI values, which correspond to magnetization values from 0 to ~7 Am^{-1}. Iterative reweighting inversion focusing (Portniaguine and Zhdanov, 2002) was applied (two iterations) to enhance susceptibility contrasts and the localization of high susceptibility bodies. Only induced magnetization was assumed, as usual for cases when the origin and age of anomalies is uncertain (e.g., Neres et al., 2018).

We provide the two output 3D inversion models (susceptibility voxi) as supplementary files S3 and S4 as XYZ ascii files.

Results from the inversion modeling are represented in Figure 15. The output voxi were clipped for high susceptibility values, as described in the figure. Geographical clipping was also performed to discard areas that were not surveyed, especially near the coast of Sines and to the west of the Côvo anomaly. This ensures that the interpreted bodies are confidently constrained by data. The shown bottom of the Côvo body was restricted to 13.3 km. The Sines, Côvo and Milfontes anomalies are inverted as high susceptibility bodies that clearly stand out from the rest of the volume. Note that these models do not intend to represent the geometry and parameters of the real bodies but are mostly indicative and comparative.

Table S1.

Marine magnetic surveys considered for this work. Refer to Figure 2 for location of survey lines.

R/V Selvagem Grande, owned by the Portuguese Task Group for the Extension of the Continental Shelf, EMEPC: https://www.emepc.pt/embarcacao-selvagem-grande?lang=en

R/V Noruega, owned by IPMA, decommissioned: https://www.ipma.pt/en/navios/noruega/

R/V Diplodus, owned by IPMA: https://www.ipma.pt/en/navios/diplodus/

Survey	Dates interval	Nº survey days	Research Vessel	Base station for diurnal correction
ROCHEL-1	10/10/2014 - 24/10/2014	6	Selvagem Grande	Coimbra
ROCHEL-2	24/06/2015 - 10/07/2015	9	Selvagem Grande	Coimbra
CHELSI	24/04/2018 - 28/04/2018	4	Selvagem Grande	São Teotónio
MINEPLAT-1	07/10/2016 - 16/10/2016	10	Noruega	São Teotónio
MINEPLAT-2	31/03/2017 - 08/04/2017	9	Diplodus	Toledo
MINEPLAT-3	08/06/2018 - 18/06/2018	11	Noruega	São Teotónio
MINEPLAT-5	10/03/2019 - 31/03/2019	16	Noruega	São Teotónio
	Total	65		

File S1. Coordinates (longitude, latitude) of the polygon delimiting the offshore outcropping rocks of the Sines magmatic complex, as mapped in Figure 11.

File S2. Coordinates (longitude, latitude) of the polygon delimiting the Jurassic sedimentary rocks outcropping offshore north of the Sines igneous complex, as mapped in Figure 11.

File S3. Output 3D inversion susceptibility model (voxi) for the Sines-Côvo area, as XYZ file. See Text S2.

File S4. Output 3D inversion susceptibility model (voxi) for the Milfontes area, as XYZ file. See Text S2.

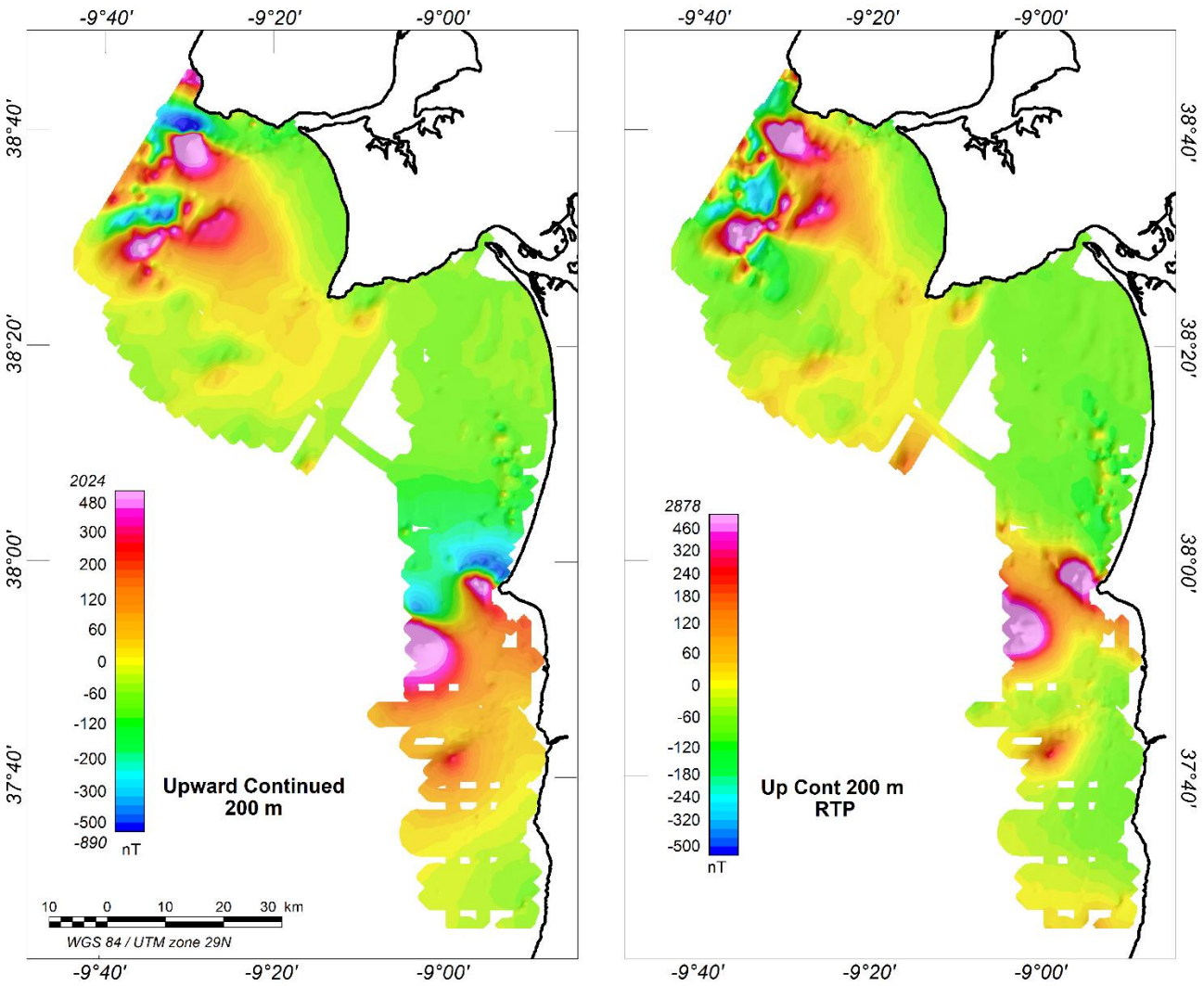

Figure S1. Magnetic anomaly upward continued to 200 m height, and respective reduction to the pole.

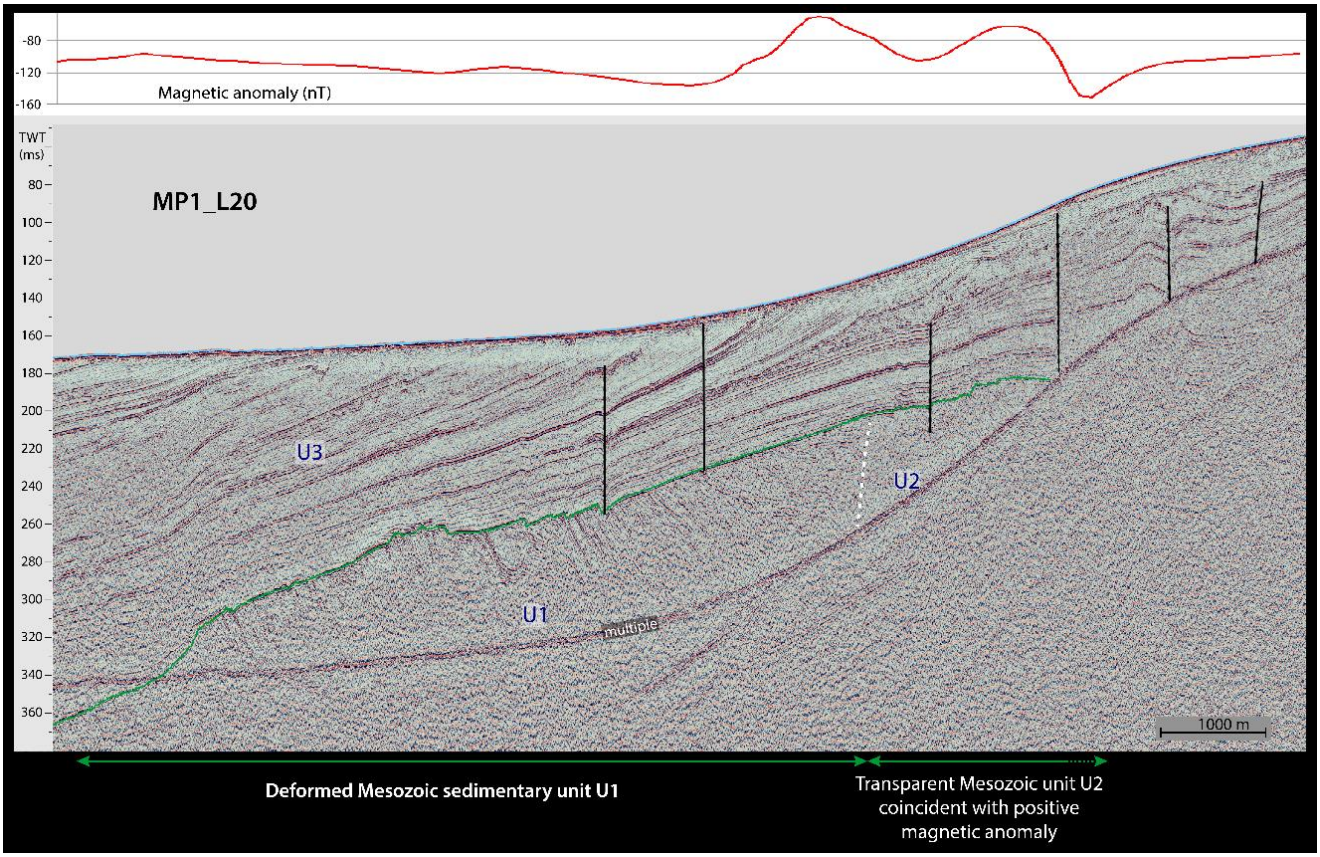

Figure S2. Seismic interpretation of the Mineplat MCS line MP1_L20. Refer to Figure 13a for location.

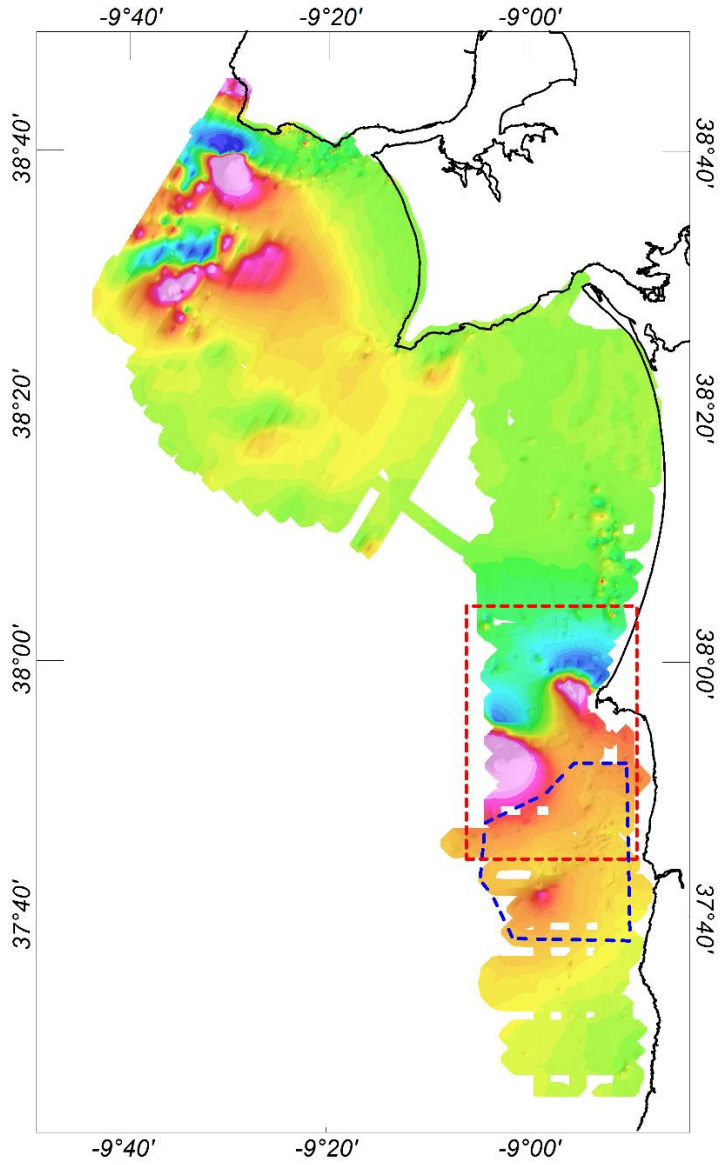

Figure S3. Polygons defining the areas used for 3D magnetic inversion (Figure 15). Red: for Sines and Côvo anomalies; blue: for Milfontes anomaly. C.f. Supplementary Text S2.

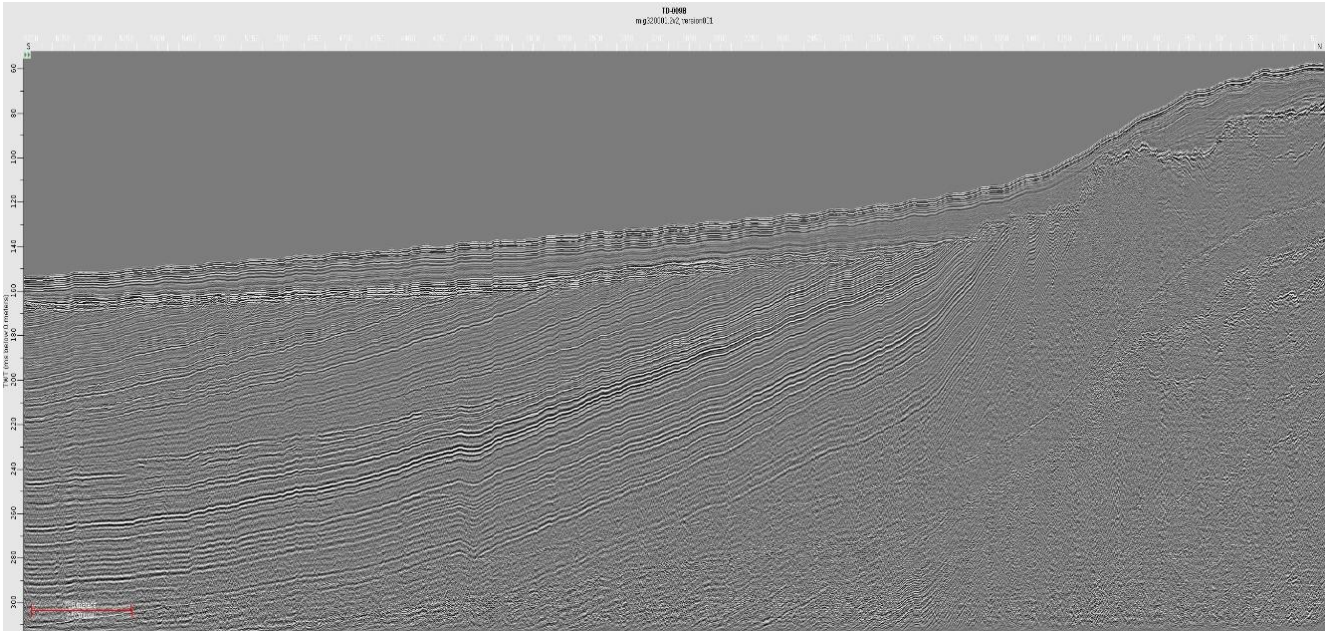

Figure S4. Non-interpreted seismic line TD_09B.

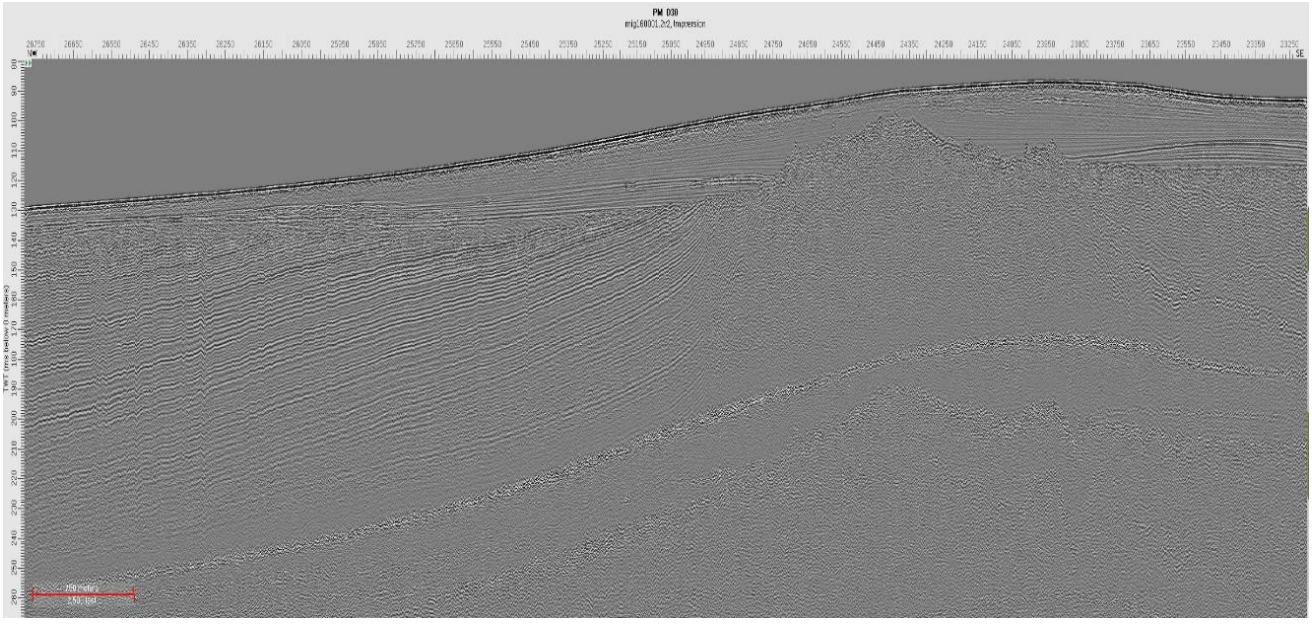

Figure S5: Non-interpreted seismic line PM_D30.

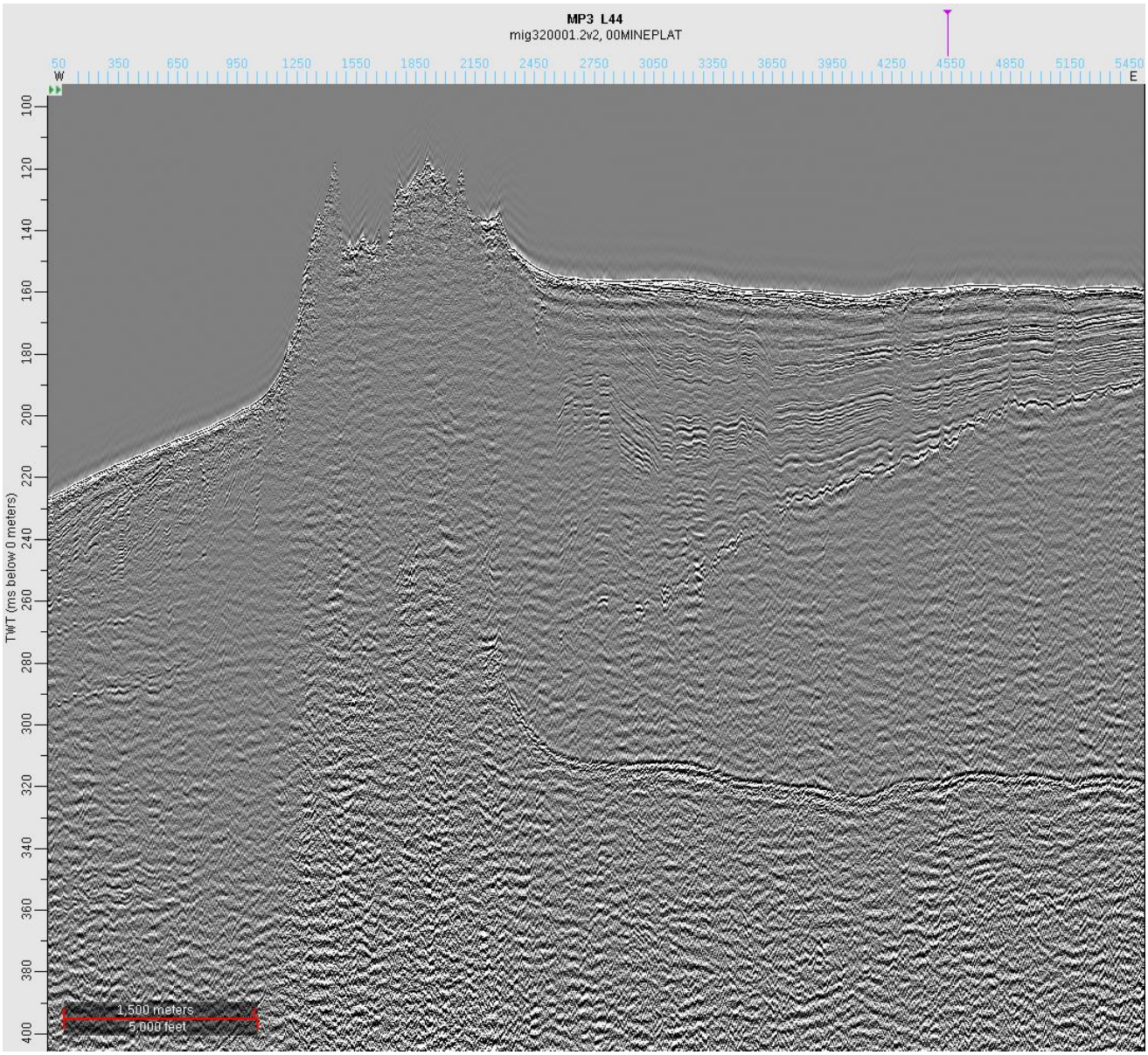

Figure S6: Non-interpreted seismic line MP3_L44.

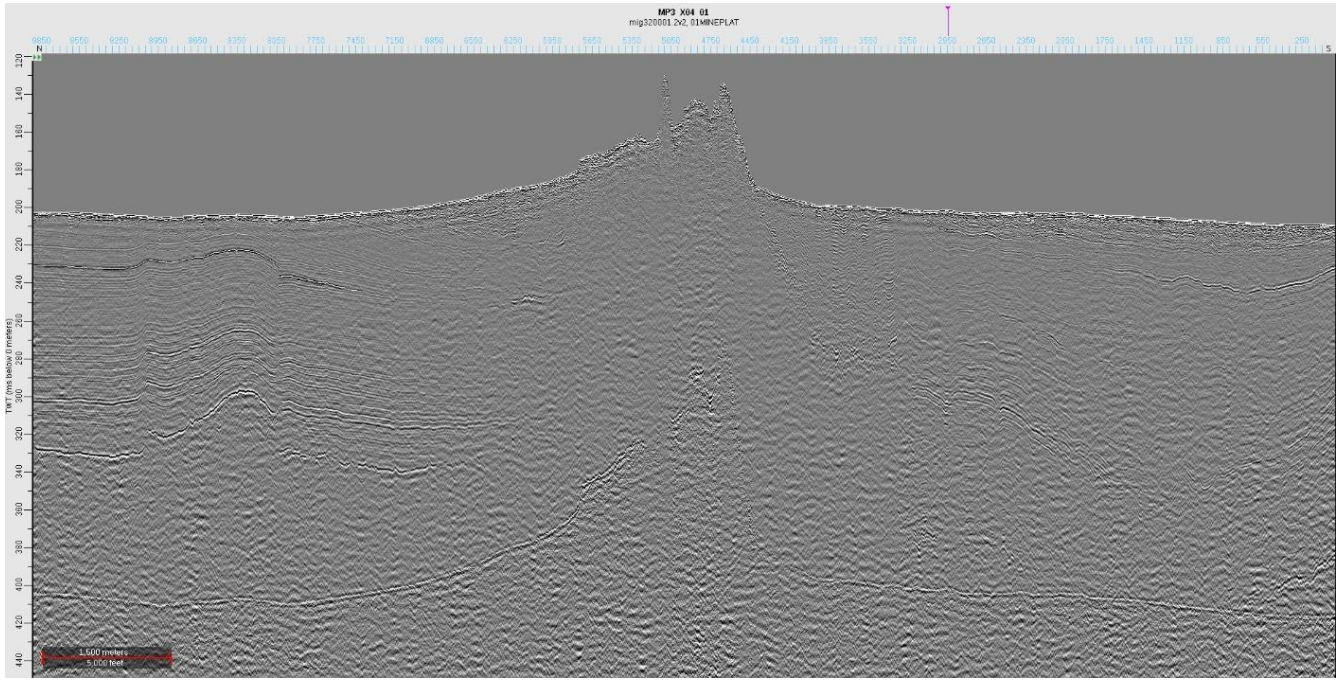

Figure S7: Non-interpreted seismic line MP3_X04.

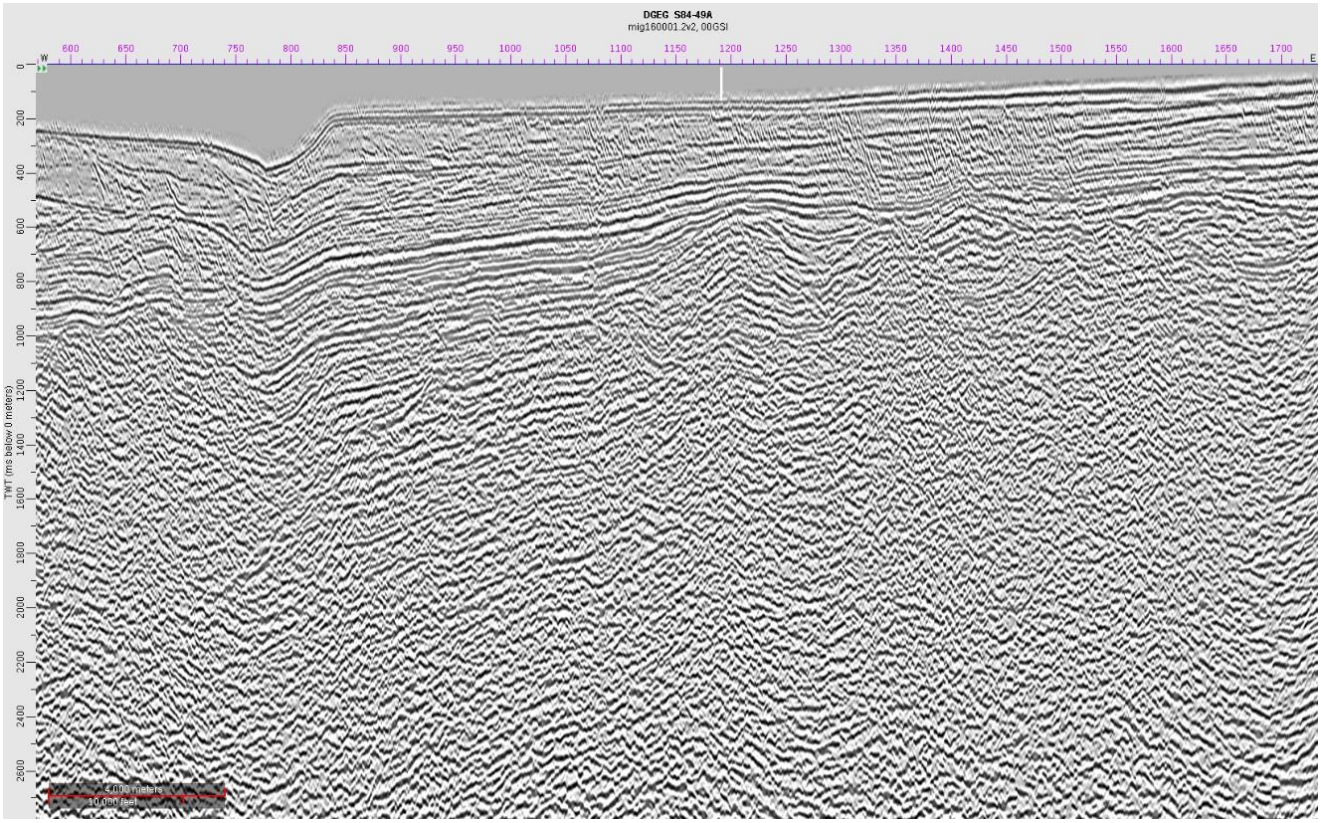

Figure S8: Non-interpreted seismic line GSI-49.

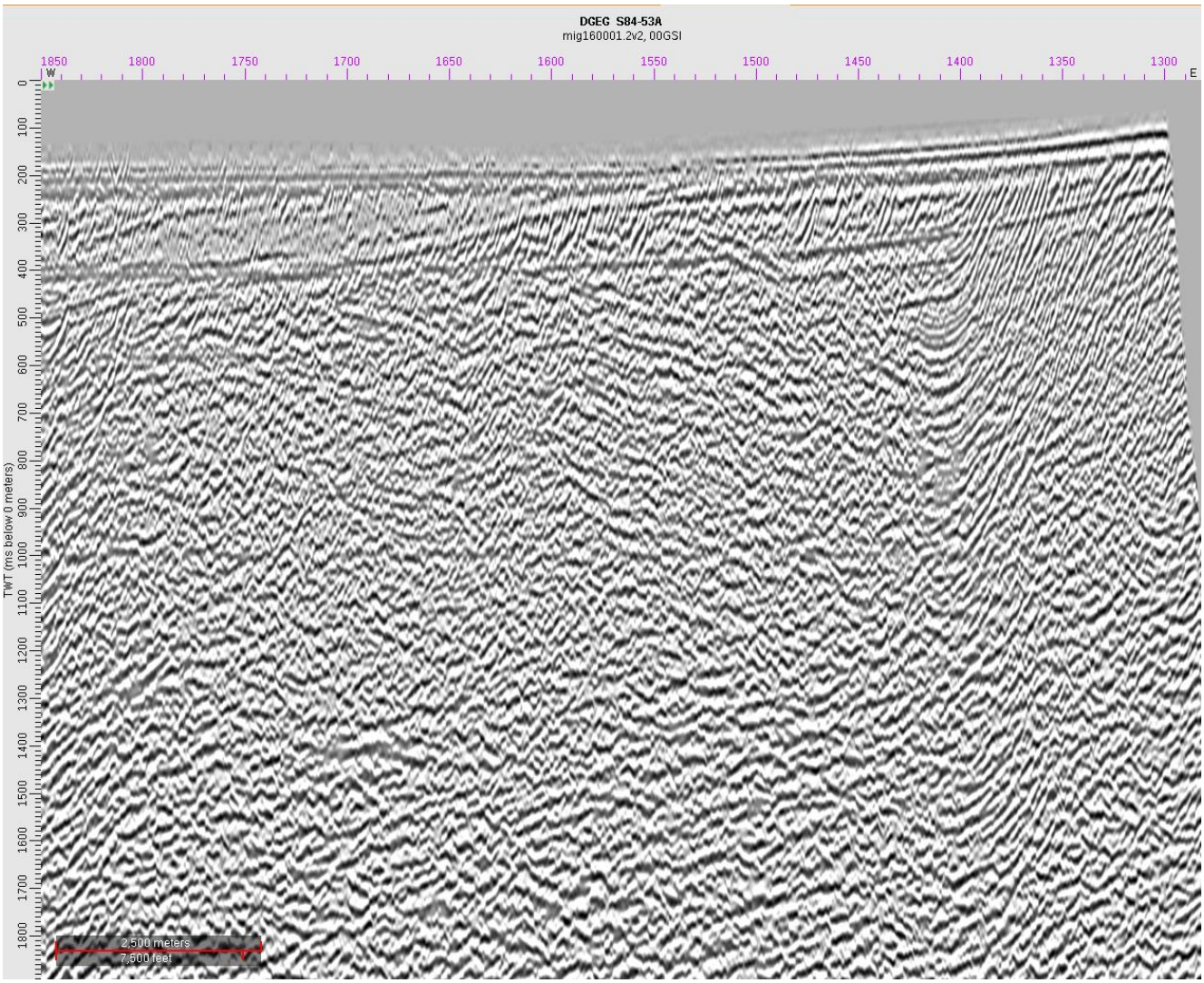

Figure S9: Non-interpreted seismic line GSI-53A.

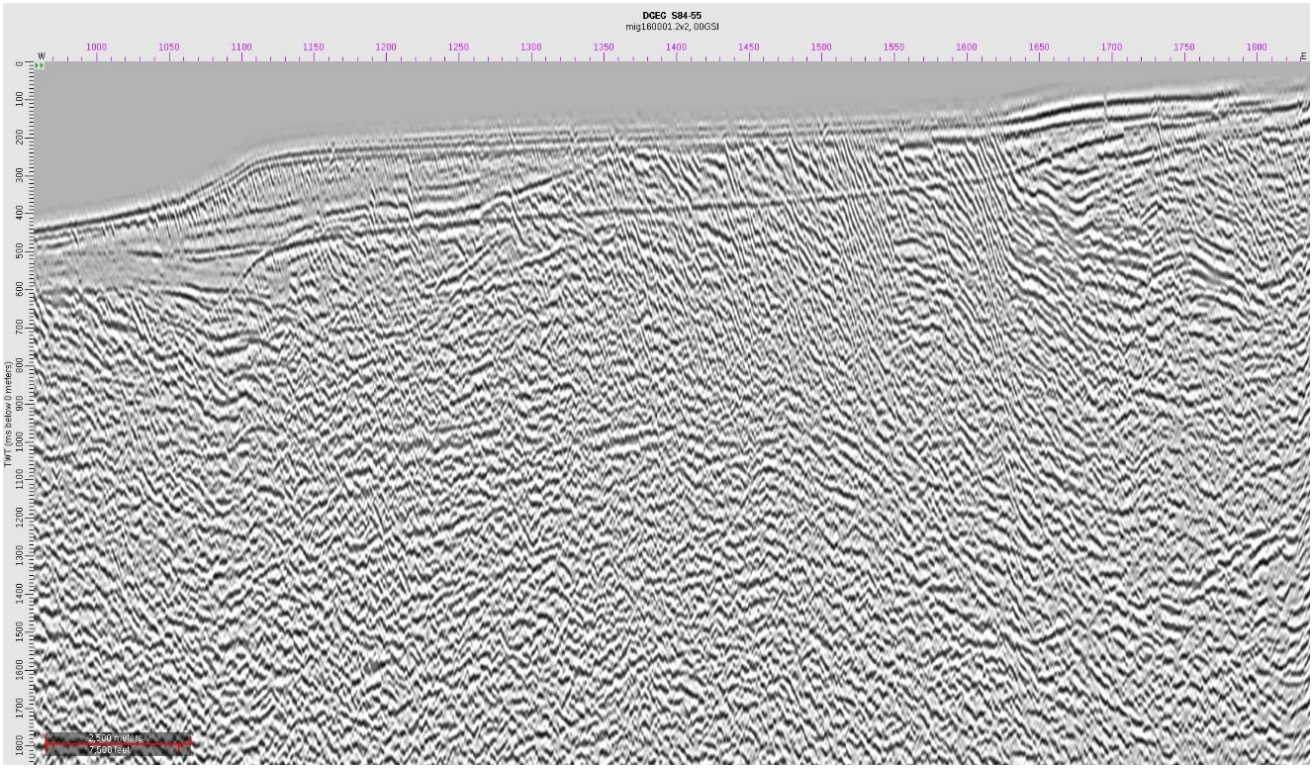

Figure S10: Non-interpreted seismic line GSI-55.

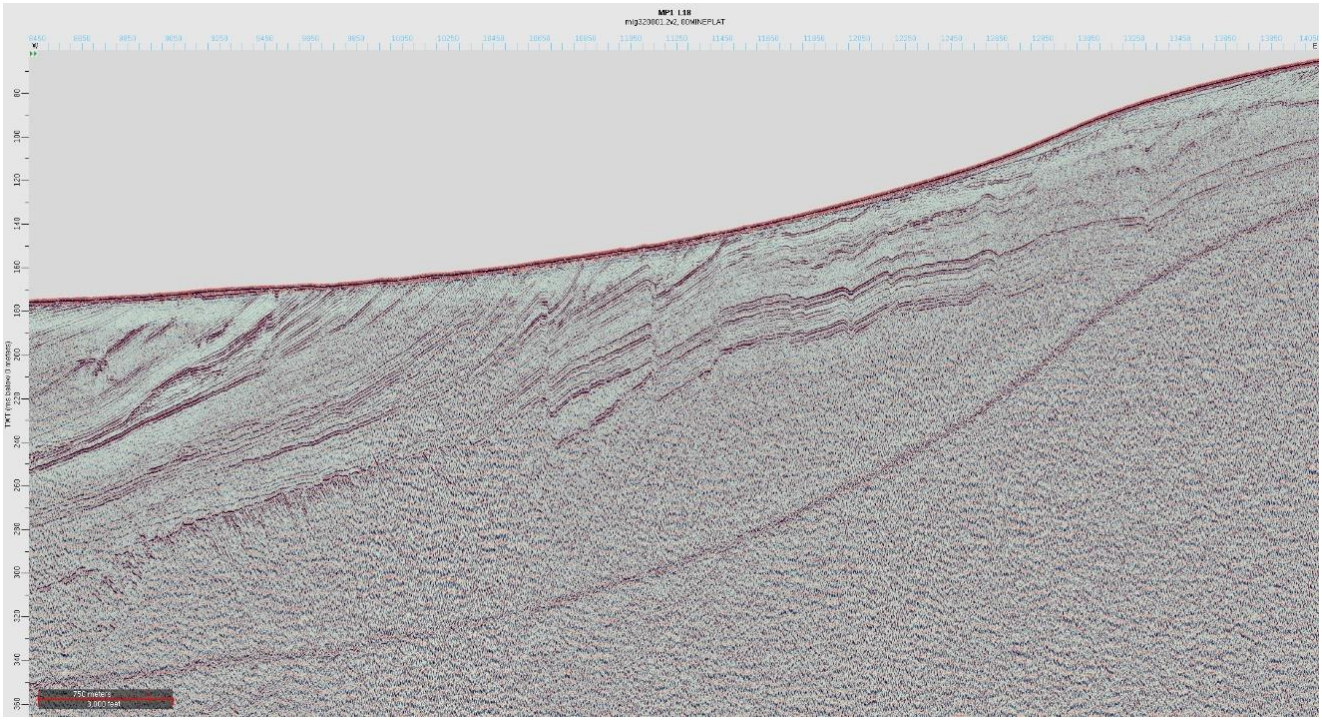

Figure S11: Non-interpreted seismic line MP1_L18.

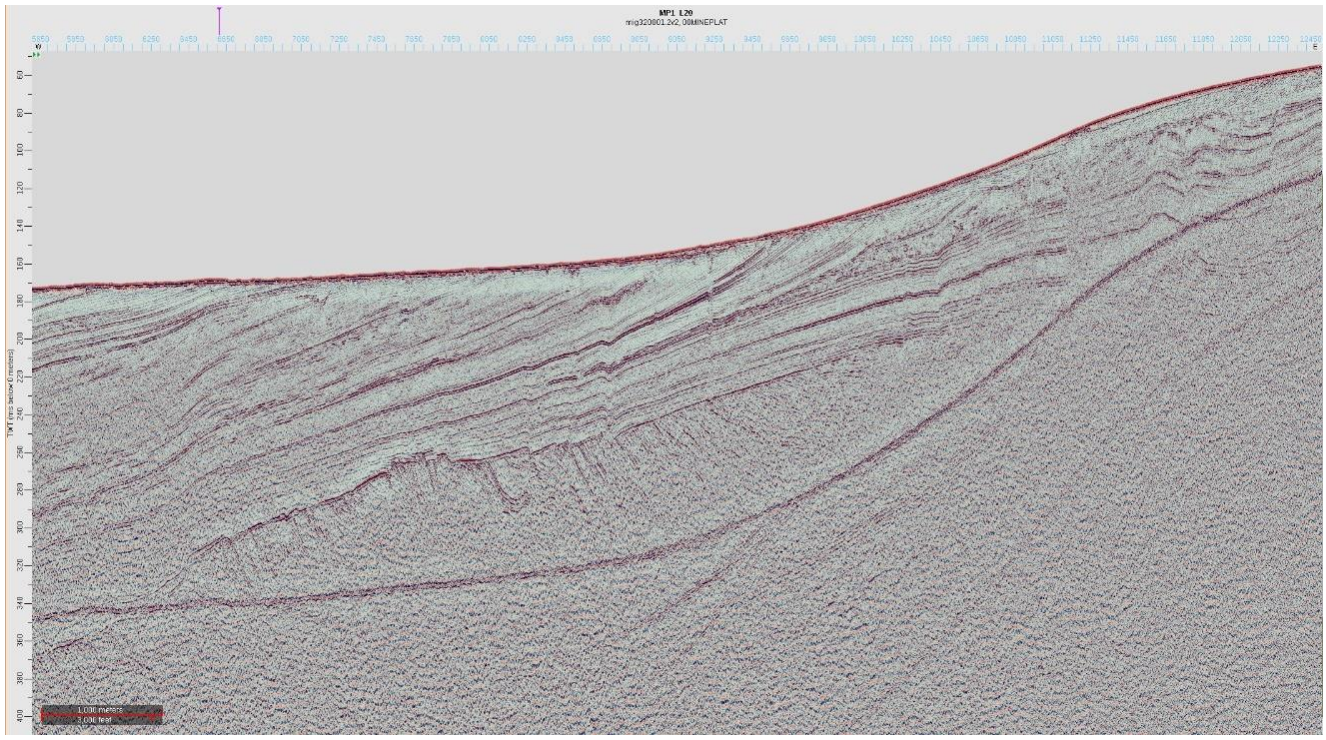

Figure S12: Non-interpreted seismic line MP1_L20.

References

Neres, M., Terrinha, P., Custódio, S., Silva, S. M., Luis, J., & Miranda, J. M. (2018). Geophysical evidence for a magmatic intrusion in the ocean-continent transition of the SW Iberia margin. Tectonophysics, 744. https://doi.org/10.1016/j.tecto.2018.06.014

Ellis, R. G., de Wet, B., & Macleod, I. N. (2012). Inversion of magnetic data for remanent and induced sources. In ASEG Extended Abstracts, pp. 1-4.

Portniaguine, O., & Zhdanov, M. S. (2002). 3-D magnetic inversion with data compression and image focusing. Geophysics, 67(5), 1532–1541. https://doi.org/10.1190/1.1512749